NAVAL POSTGRADUATE SCHOOL
MONTEREY, CALIFORNIA

THESIS

COMPARATIVE COMPUTATIONAL ANALYSIS
OF
AIRFOIL SECTIONS FOR USE ON SAILING CRAFT

by

Louis P. Partida

March, 1996

Thesis Advisor: Garth V. Hobson

Approved for public release; distribution is unlimited.

DISCLAIMER NOTICE

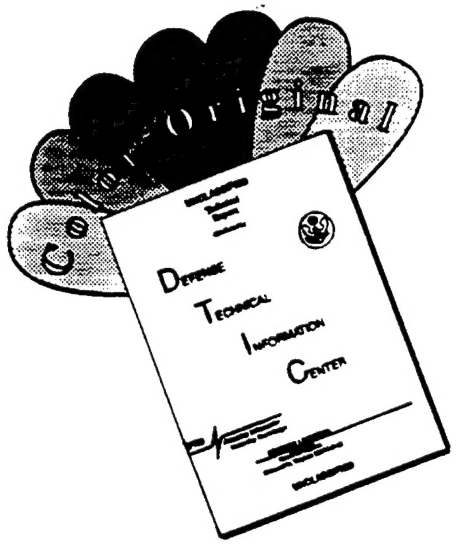

THIS DOCUMENT IS BEST QUALITY AVAILABLE. THE COPY FURNISHED TO DTIC CONTAINED A SIGNIFICANT NUMBER OF COLOR PAGES WHICH DO NOT REPRODUCE LEGIBLY ON BLACK AND WHITE MICROFICHE.

REPORT DOCUMENTATION PAGE

Form Approved OMB No. 0704-0188

1. AGENCY USE ONLY *(Leave blank)*	2. REPORT DATE March 1996	3. REPORT TYPE AND DATES COVERED Master's Thesis

4. TITLE AND SUBTITLE COMPARATIVE COMPUTATIONAL ANALYSIS OF AIRFOIL SECTIONS FOR USE ON SAILING CRAFT

5. FUNDING NUMBERS

6. AUTHOR(S) Louis P. Partida

7. PERFORMING ORGANIZATION NAME(S) AND ADDRESS(ES)
Naval Postgraduate School
Monterey CA 93943-5000

8. PERFORMING ORGANIZATION REPORT NUMBER

9. SPONSORING/MONITORING AGENCY NAME(S) AND ADDRESS(ES)

10. SPONSORING/MONITORING AGENCY REPORT NUMBER

11. SUPPLEMENTARY NOTES The views expressed in this thesis are those of the author and do not reflect the official policy or position of the Department of Defense or the U.S. Government.

12a. DISTRIBUTION/AVAILABILITY STATEMENT
Approved for public release; distribution is unlimited.

12b. DISTRIBUTION CODE

13. ABSTRACT *(maximum 200 words)*

This thesis represents the results of a comparative analysis of current and proposed airfoil sections for use on sailing craft. The primary goal of this report is to develop a sail replacement that functions with the ease and durability of current sailboat sails, yet offers a marked improvement in overall performance, with minimum penalties of weight and construction complexity. State-of-the-art computational methods are utilized to determine the respective aerodynamic characteristics of a model of a current windsurfer sail section and models of a proposed semi-rigid wing-sail section. Wing-sails offer the same promise of performance gains that modern airfoils have produced in comparison to early thin airfoils. An investigation into differences and possible benefits of the analyzed sections' aerodynamic loading and stall characteristics is made using fully viscous Navier-Stokes Computational Fluid Dynamic codes. Finally a full three-dimensional wing-sail computational model is constructed to identify further areas where sectional improvements would enhance the overall performance of the lifting shape.

14. SUBJECT TERMS Windsurfing, sail design, computational fluid dynamics, CFD, grid generation, GRIDGEN, OVERFLOW, FAST, NS, Navier-Stokes.			15. NUMBER OF PAGES 68 16. PRICE CODE
17. SECURITY CLASSIFICATION OF REPORT Unclassified	18. SECURITY CLASSIFICATION OF THIS PAGE Unclassified	19. SECURITY CLASSIFICATION OF ABSTRACT Unclassified	20. LIMITATION OF ABSTRACT UL

NSN 7540-01-280-5500

Standard Form 298 (Rev. 2-89)
Prescribed by ANSI Std. 239-18 298-102

Approved for public release; distribution is unlimited.

COMPARATIVE COMPUTATIONAL ANALYSIS OF AIRFOIL SECTIONS FOR USE ON SAILING CRAFT

Louis P. Partida
Lieutenant, United States Navy
B.S., United States Naval Academy, 1986

Submitted in partial fulfillment
of the requirements for the degree of

MASTER OF SCIENCE IN AERONAUTICAL ENGINEERING

from the

NAVAL POSTGRADUATE SCHOOL
March 1996

Author: _____
Louis P. Partida

Approved by: _____
Garth V. Hobson, Thesis Advisor

_____
Richard M. Howard, Second Reader

_____
Daniel J. Collins, Chairman
Department of Aeronautics and Astronautics

ABSTRACT

This thesis represents the results of a comparative analysis of current and proposed airfoil sections for use on sailing craft. The primary goal of this report is to develop a sail replacement that functions with the ease and durability of current sailboat sails, yet offers a marked improvement in overall performance, with minimum penalties of weight and construction complexity. State-of-the-art computational methods are utilized to determine the respective aerodynamic characteristics of a model of a current windsurfer sail section and models of a proposed semi-rigid wing-sail section. Wing-sails offer the same promise of performance gains that modern airfoils have produced in comparison to early thin airfoils. An investigation into differences and possible benefits of the analyzed sections' aerodynamic loading and stall characteristics is made using fully viscous Navier-Stokes Computational Fluid Dynamic codes. Finally a full three-dimensional wing-sail computational model is constructed to identify further areas where sectional improvements would enhance the overall performance of the lifting shape.

TABLE OF CONTENTS

I. INTRODUCTION

A. BACKGROUND

As in the field of aircraft design, the development of sails for high performance sailboats has traditionally benefitted from the technology transfer from high expenditure programs such as America's Cup Yacht development efforts. Unfortunately, the majority of sailmakers and designers have had little access to the powerful engineering and design tools that encompass today's aerospace engineering field (Figure 1.1), mostly because of

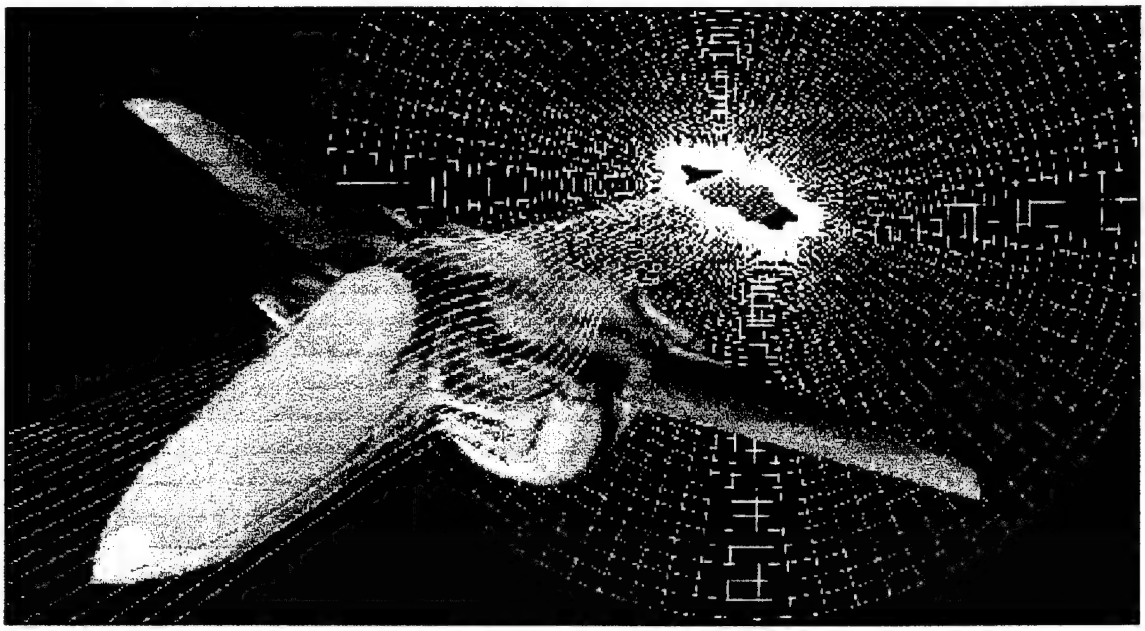

Figure 1.1 - Example of Current CFD Flowfield Investigations.

the huge cost involved. Without this access sail designers have had to rely on experience and the trial-and-error method of testing sail shapes in the sport of sailboat racing [Ref. 1]. This trend is starting to change, due largely to the evolution of the personal computer (PC). Improvements in power, speed, and memory of PC's have made design tools that once were only available to research scientists and design engineers, accessible to today's

sailboat designers. Already many designers are utilizing computer-aided drawing and drafting programs and some sail makers are touting the benefits of their own sail design software (Figure 1.2) and computer-guided cutting tools. Many designers expect more rapid advancements in these fields, making these resources more affordable and available to a wider market [Ref. 2].

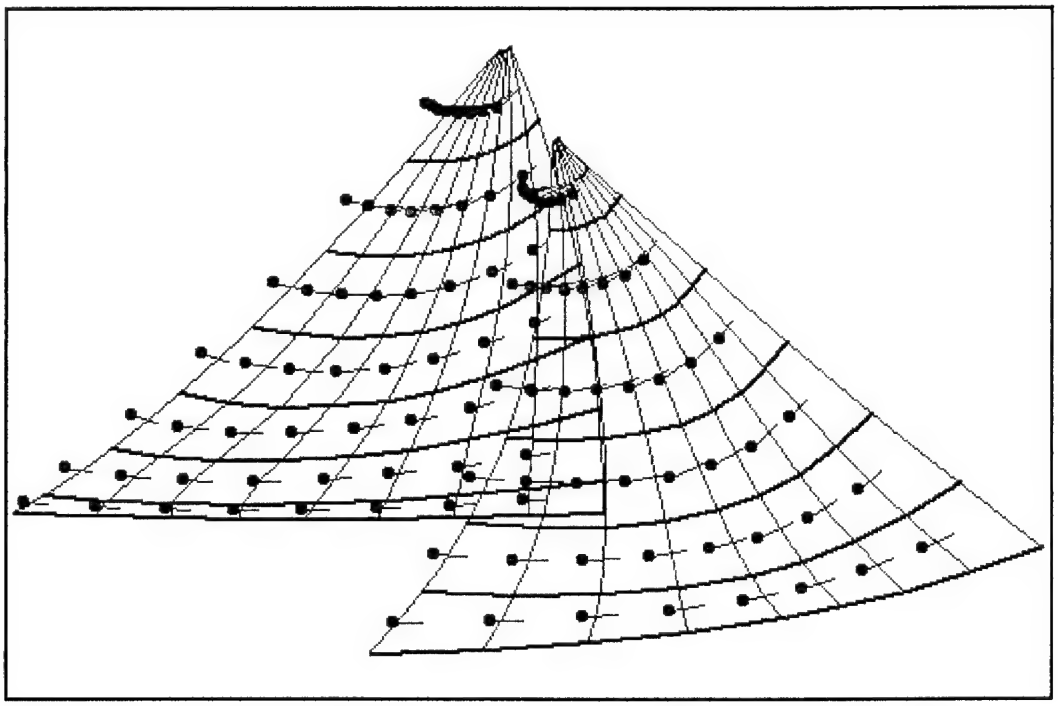

Figure 1.2 - Example Output from a Commercial Panel Code (Macsail) for the Analysis of Sails, by WB-Sails of Finland .

Except for a few individual efforts in academia and the highest level of sailboat racing, little attention has been paid to the possible benefits of computer analysis of the flow fields about sails and the ensuing optimization of these shapes. Again due to limitations of computer resources, the majority of these investigative efforts have focused on inviscid and/or potential flows about sails [Refs. 3,4, 5, and 6]. Recently

another Naval Postgraduate School student [Ref. 7] presented a thesis that not only covered the Computational Fluid Dynamic (CFD) analysis of viscous and turbulent flow about a sail section, but he also validated his findings with experimental data from a wind tunnel model. All his computational analyses were performed using a desktop Unix workstation, which demonstrated the accessibility and usability of this technology throughout the sailing industry. In the three years since the presentation of this work, computer technology has continued to advance and now desktop PCs rival the power of very expensive workstations, making this technology even more affordable.

In concert with advances in computer technology there has been the proliferation of the use of wings as the driving force of sailboats, which when properly utilized can clearly outperform "soft sails" [Ref. 8]. The advantages of using wings for sailboat propulsion were demonstrated in the 1988 winged catamaran defense of the America's Cup and more recently by the success of an American team at the International Catamaran Challenge Trophy (ICCT or Little America's Cup). This race is contested in C-class catamarans, a fairly open design platform, limiting the boats to thirty feet of length, fourteen feet of width, and three hundred square feet of sail area; everything else is unrestricted. Since the late 1960's these boats have utilized various forms of rigid wings for sails [Ref. 6]. The 1996 winner, Team Cogito, utilized a three-element high-aspect-ratio wing on a rotating mast, using the latest in carbon fiber technology (Figure 1.3). Like the performance improvements from the "big" America's Cup, experts expect the very latest in wing technology from the ICCT to trickle-down to all sailboat designs [Ref. 9]. Although rigid wing-sails have come a long way, they still suffer from being

complex and structurally fragile in most conditions. These limitations typify why wing-sails have yet to be widely used for general recreational sailboats.

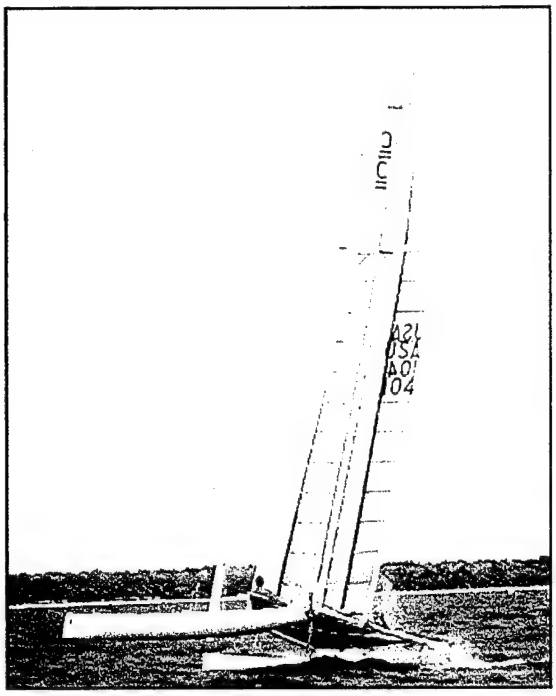

Figure 1.3 - the 1996 ICCT Winner, Cogito, with Her Three-element Wing-sail in its Upwind Configuration (Photo by Richard Gladwell).

B. PURPOSE AND PROBLEM

This thesis entails an attempt to optimize current sail shapes by inserting a basic symmetrical airfoil into a previously generated model of current sail sections [Ref. 7]. The primary purpose of the ensuing computational investigation was to produce a more efficient lifting shape to be used as a simple sail replacement. Some of the goals for this new shape were to design a sail that is lightweight, durable, easy to use, and at the same time produce a marked increase in performance.

Although the latest sport sailboats offer a big performance improvement over traditional designs, the platform that offers the simplest sailplan while pushing the boundaries of sail-powered performance continues to be the windsurfer. The windsurfer sail (Figure 1.4) offers many advantages as a model for computational analysis. The most obvious advantage to this choice is the simplicity of the design. Reflecting a moderate aspect-ratio wing, the single sail simply slips over the mast, eliminating the

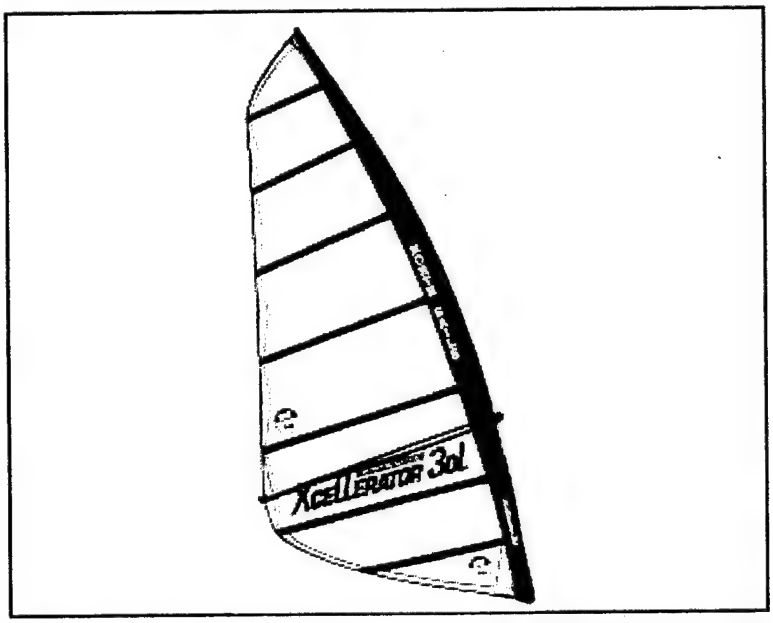

Figure 1.4 - Example of a Current Windsurfer Sail Planform (from North Sails Catalog).

interaction of multiple sails and supporting wires such as those found on the more common sloop rig. Since the shape of the windsurfer sail can not be readily adjusted while sailing, the sail must be designed for the predominate conditions, and although the shape proposed in this thesis is a semi-rigid wing design, its use of standard materials and sail controls will give it both durability, and the ability to be adjusted for a wide range of sailing conditions.

It is the predominate aerodynamic operating conditions of sailboat sails that make the computational analysis of these lifting surfaces challenging. The majority of CFD work to date has been confined to flight regimes described by Reynolds numbers (Re) above one million. Analyses conducted at lower Re's have been generally restricted to internal flows. Although windsurfers operate at faster speeds than the average sailboat, the Reynolds number is still very low, indicating a large influence from viscous forces. At such slow aerodynamic speeds the flow field is assumed to be incompressible. Also current construction techniques and the materials used for sails, especially the mast pocket, cause many imperfections and rough surfaces, allowing the further assumption of fully turbulent flow [Ref. 7].

The conditions used for this analysis are based on the windsurfer having already accelerated to hull planing speed. Figure 1.5 shows an example of two different sailing conditions encountered; broad-reaching and close-reaching. Assuming the hull is planning at 30 Kts for both cases, the close-reach condition yields a propulsive force equal to only about 47% of the lift force generated by the sail whereas in the broad-reach scenario the propulsive force is approximately 101% of the lift generated by the sail. Of note in these different situations is the radical difference in the apparent wind, the wind that the sail actually feels. In the close-reach condition 30 Kts of true wind speed coupled with the hull speed generates approximately 42 Kts of apparent wind. While on a broad-reach approximately 48 Kts of true wind are needed to generate only 30 Kts of apparent wind. This clearly shows that although directing the aerodynamic force along the desired course should provide the most efficient use of the sail's power, it requires

very high wind to generate enough apparent wind to attain record setting speeds. Currently most windsurfers require a minimum of 15 Kts of true wind speed on a close-reach to attain hull planning speed (approximately 12 Kts) [Ref. 10].

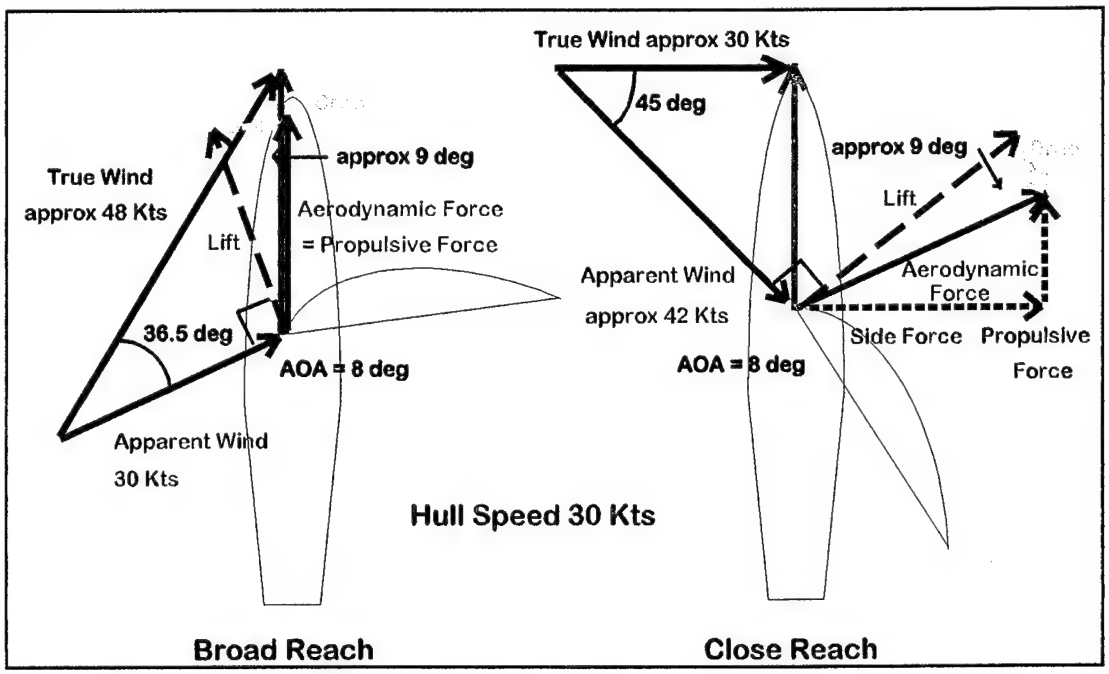

Figure 1.5 - Example of Wind Velocity and Aerodynamic Force Relationships for Two Modes of Sailing.

Although the majority of this analysis only deals with the two-dimensional characteristics of sail sections, the ultimate goal is to construct a full three-dimensional computer model of a wing-sail for use on a windsurfer. This requires an attempt to model the actual conditions found while sailing, including the interaction of the wind/water boundary layer effect. This boundary layer effect creates a velocity profile that is very similar to the ones produced by boundary layers seen over aerodynamic surfaces in a flowfield. This atmospheric boundary layer not only affects the true wind velocity but also the apparent velocity and wind angle as a function of height above water.

This true wind velocity boundary layer profile can be approximated by:

$$V_T(z) = V_{T_{REF}} \log\left(\frac{z}{z_{REF}}\right)^{\omega} \quad \text{[Ref. 6]}$$

Where: $V_T(z)$= true wind velocity as a function of heigth above water (z).

$V_{T_{REF}}$ = a designated true wind velocity at a reference height above water.

z_{REF}= a reference length dependent on the reference true wind height.

ω = surface roughness parameter (for wind over smooth surface $\omega = 1.4$).

Applying the above conditions of close and broad reaching, the effects of this boundary layer can be plotted along the mast height of a typical windsurfer sail (Figure 1.6). A table of the respective calculations are presented in Appendix A. Since the course and

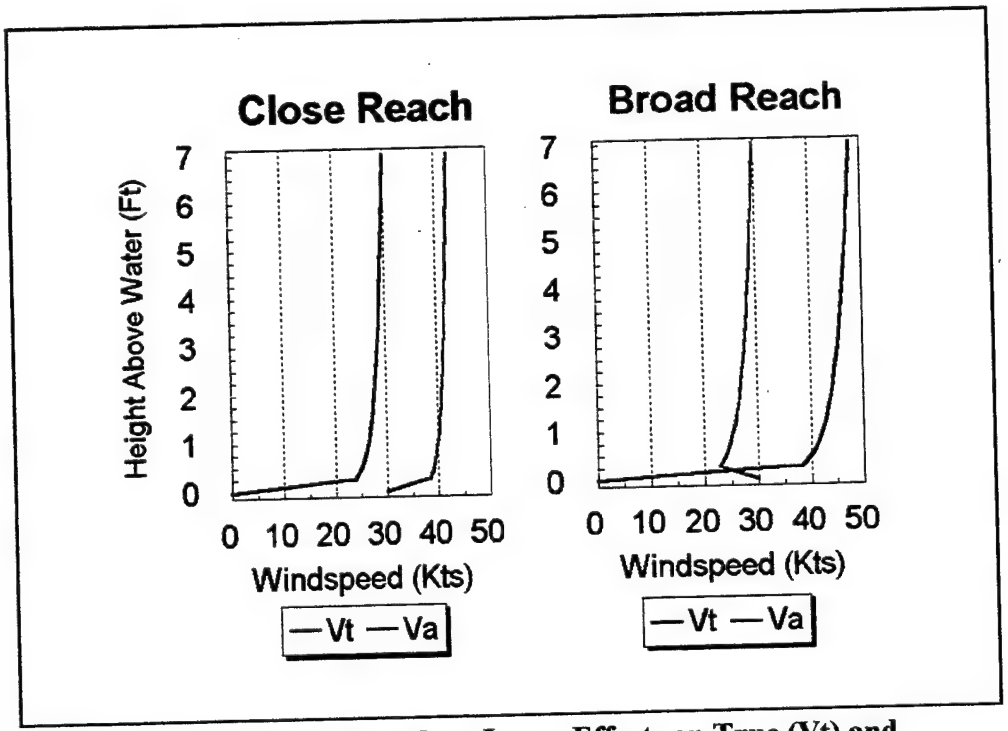

Figure 1.6 - Example of Boundary Layer Effects on True (Vt) and Apparent (Va) Wind Velocity for Two Modes of Sailing.

speed are held constant, the apparent wind velocity profile results in a apparent wind angle shift along the mast length (Figure 1.7). Traditional sailors have always used the standard controls of halyard tension, outhaul tension, and/or sheet adjustment to shape their sail for optimum flow over its surface along the entire mast height in order to

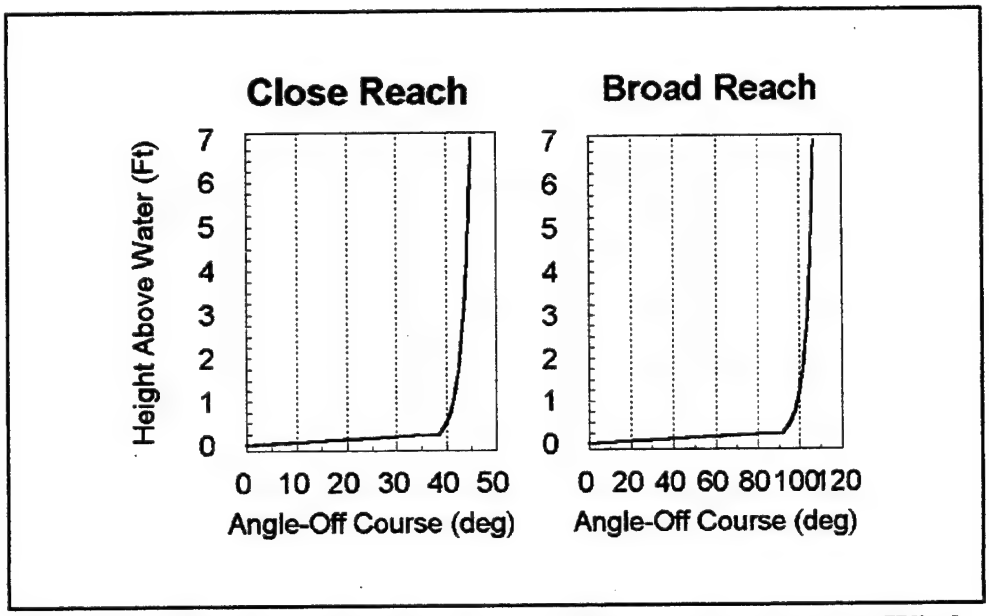

Figure 1.7 - Example of Boundary Layer Effects on the Apparent Wind Angle for Two Different Modes of Sailing

garnish the most performance (i.e. constant relative angle of attack). This has always resulted in a considerable amount of 'twist' in the sail at the top (head) as compared to the bottom (foot). It is because of this phenomenon of apparant wind shift that designers of wing-sails have been striving for the ability to warp or 'twist' their shapes [Ref. 9]. Since the proposed wing-sail will be constructed from standard sail material and use traditional controls, its ability to twist should be akin to that of a traditional sail.

II. COMPUTATIONAL ANALYSIS

A. GENERAL

Computational Fluid Dynamics (CFD) is the prediction of fluid flows by numerical solution of the equations of motion. By solving these equations for a specified shape within a flowfield, CFD can be used in the design process of many fluid flow systems [Ref. 11]. The past two decades have seen a remarkable surge in the

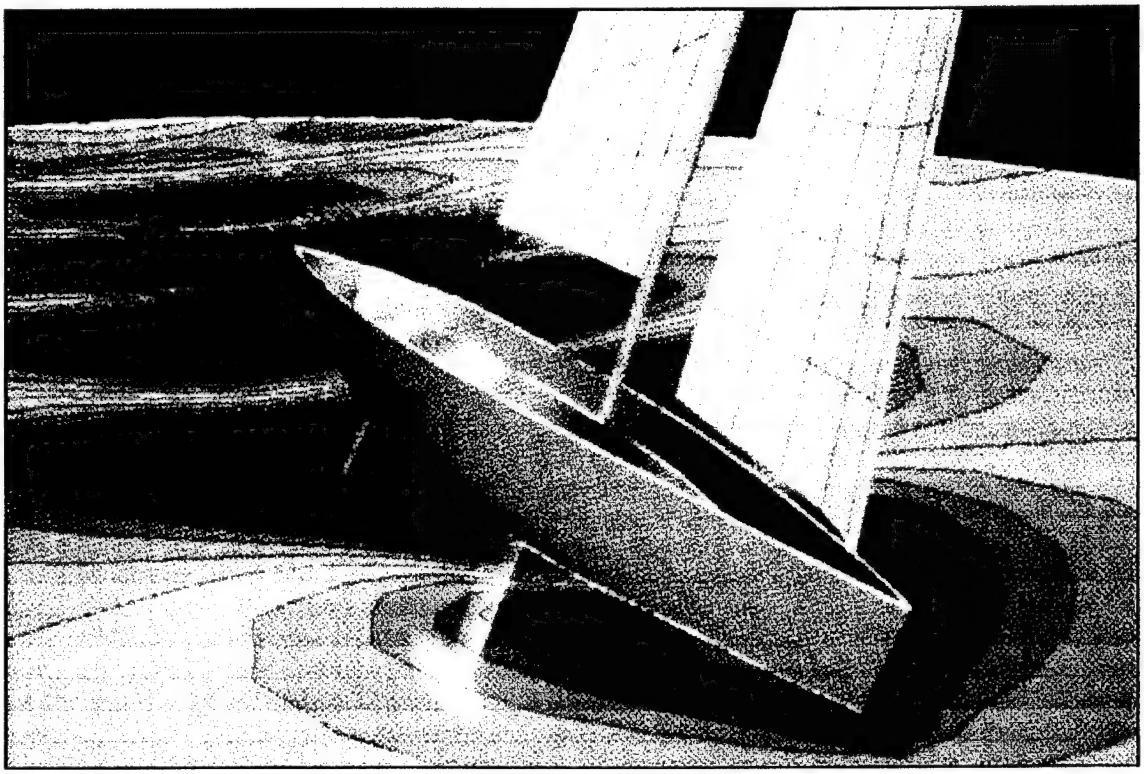

Figure 2.1 - Example of CFD Program for Yacht Design "Splash" by South Bay Simulations (Graphic from *Sailing World*, January 1996).

development of numerical schemes designed to solve these equations, achieving higher convergence rates, and improving the stability of the solution. When utilized, CFD has

typically been used to analyze hull and keel designs as a cost saving measure prior to the tank testing of models, much the same way it is used in the aerospace industry [Ref. 12].

Until more recently these CFD techniques were not seriously used to analyze the flow about sails, largely because of the very unsteady nature of the flow field and the inability to accurately model the interaction between the various components of sailing rigs; multiple sails, masts, shroud lines, etc. [Ref. 3]. While the technology to apply this analysis method has become more accessible, the perception that increasing the driving capability of a yacht's sails is equally if not more important as decreasing the drag of its hull, has put new emphasis on sail design. Now, in conjunction with new sailmaking technologies and methods such as North Sail's 3DL molded sail techniques, CFD analysis can be used to refine traditional sail shapes and identify areas of lost performance due to excessive drag or flow separation.

The following analysis demonstrates a capability now available to all sailmakers and designers for analyzing sail designs using the latest technology of fully viscous flowfield simulation. This CFD analysis procedure can be broken down into several basic steps: grid generation, flow solution, flow visualization, quantitative and qualitative analysis. It quickly becomes an iterative process as the solution is judged to be acceptable or not, and if not, a decision must be made to change/refine the grid, or change the input parameters for the flow solver (see Figure 2.2). If the solution "looks" reasonable other factors must be weighed to determine if the solution is realistic, or physical. These factors include inspecting the force and moments, the pressure distribution, velocity profiles, and comparisons with available experimental data and theoretical criteria.

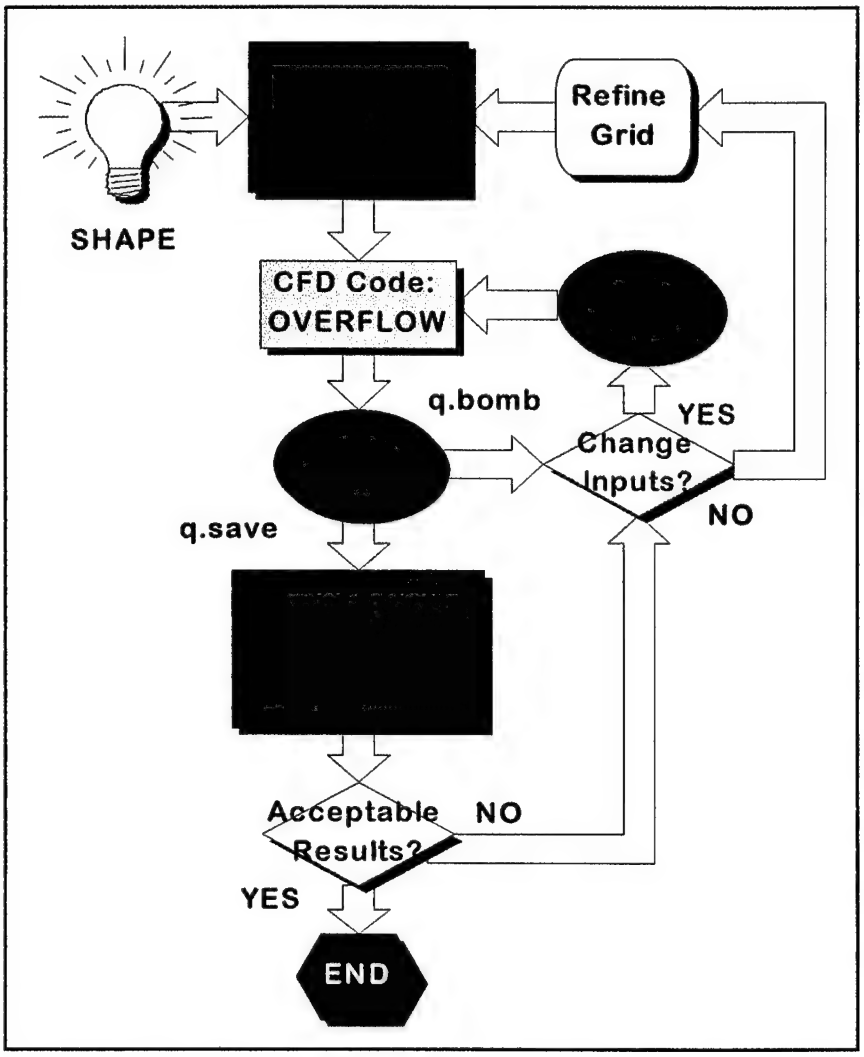

Figure 2.2 - Flowchart Illustrates the CFD Analysis Procedure

B. NAVIER-STOKES METHOD

By selecting equations that describe the flowfield, discretizing them, and applying a proper numerical procedure to a specified geometry, many flowfields can be simulated and analyzed using current CFD techniques [Ref. 11]. The conservation equations utilized to describe flowfields are the momentum equation, the energy equation and the equation of continuity. When combined these equations form the Navier-Stokes equations, which have only been accurately modeled numerically in the last three

decades. As an example the two-dimensional Navier-Stokes' equation is presented in vector form:

$$\frac{\partial Q}{\partial t} + \frac{\partial E}{\partial x} + \frac{\partial F}{\partial y} + \frac{1}{Re}\left(\frac{\partial R}{\partial x} + \frac{\partial S}{\partial y} \right) = 0$$

where the vector: $Q = [\rho, \rho u, \rho v, e]^T$

and: t is the non-dimensional time, x and y are the physical coordinates,

E and F are the inertia vectors, R and S are the stress vectors,

ρ is the fluid density, e is the total energy,

and u and v are the two-dimensional velocity components.

When certain assumptions are made concerning the flowfield (such as inviscid flow), the equations may be simplified to a form that is much easier to model, such as the Euler equations [Ref. 13].

C. COMPUTER CODES

The CFD code used for the bulk of the analysis presented here, is called OVERFLOW [Ref. 14], an implicit flow-solver developed at NASA Ames Research Center, that solves the Reynolds-Averaged Navier-Stokes equations in strong conservative form. Using an input namelist file (overflow.in) the user can define many parameters (see Appendix B for an example):

1. Basic flowfield parameters such as angle of attack, sideslip angle, Reynolds number, free-stream Mach number, and free-stream temperature.

2. Variations in the ratios of specific heats (γ), for use with internal flows.
3. Solution control parameters such as time step, Courant-Friedrichs-Levy (CFL) number limits, type of differencing scheme, and smoothing.
4. Boundary conditions applied to symmetry planes, wall boundaries, C-grid "cuts", and far-field surfaces.
5. Turbulence model type, such as the Baldwin-Lomax boundary and shear layer model and the Baldwin-Barth one equation (k) model, and where they apply;

The output from this code consists of a solution file (q.save) that defines the $\boldsymbol{Q}$ vector at each grid point, lists of the residuals (resid.out) and the force and moments (fomo.out) at each iteration, and a debugging output file (overflow.out) that lists all the input parameters used, and the maximum L_2 norm of the residuals and the grid position of this maximum residual at each iteration.

To verify the validity of the solutions obtained, another code was used as a comparison tool. This was a two-dimensional Navier-Stokes FORTRAN code [Ref. 15], that was more limited in the controls available but since it only required a single plane grid it was easier to set up (see Appendix C for the sample input). This code produced a solution file (ends.d) and surface pressure and skin friction coefficient distribution files (cp.d and cf.d respectively). The debugging output file (ns.out) gives the value of maximum density residual and its location as well as the calculated coefficients of Lift, Drag, and Moment. Although requiring considerable Central Processing Unit (CPU) time for a good solution, both codes can be run on the workstations within the Department of

Aeronautics and Astronautics computer laboratory. The NPS CRAY Y-MP EL98 was utilized for the majority of the work to reduce turn-around time.

D. GRID GENERATION

The majority of the time spent was in the creating and/or refining of grids. Four basic shapes were analyzed and grids were created for both CFD codes, requiring eight different grids. The grids for each shape were based on the same single plane grid for that shape, and spacing and grid point placement were made as standard as possible for all four shapes. Grid generation was accomplished almost entirely using a graphical interactive grid generator program, GRIDGEN Version 9, written using the Silicon Graphics Iris Graphics Library, and designed to run on Silicon Graphics 4D Series and IBM RS/6000 Series workstations [Ref. 16]. GRIDGEN, developed by Computer Sciences Corporation and sponsored by NASA ARC, is used to define three-dimensional grids about user defined bodies, allowing the placement of grid boundaries and grid points. Although not a computer-aided design (CAD) program, GRIDGEN does offer some rudimentary abilities to generate two and three-dimensional shapes, curves, and lines. Creating a grid using GRIDGEN requires several successive steps:

1. Creating or importing the desired object to be analyzed. It can be rendered in a CAD program, or if a simple geometry, can be drawn directly in GRIDGEN. The surface definition has no relationship to the grid topology or number of grid points, which can be defined independently.
2. Defining the grid outer boundary with a series of continuous segments called connectors. Grid points are placed and distributed along these segments.

3. Creating a four edged mesh grid called a domain, which may be smoothed based on user defined boundary conditions using an elliptical solver. This grid type can be used with the two-dimensional code.
4. Creating a three-dimensional grid requires grouping together six or more domains as the faces of a block volume grid (see Figure 2.3). Smoothing the blocked mesh grid about the shape if necessary, with the elliptical solver.

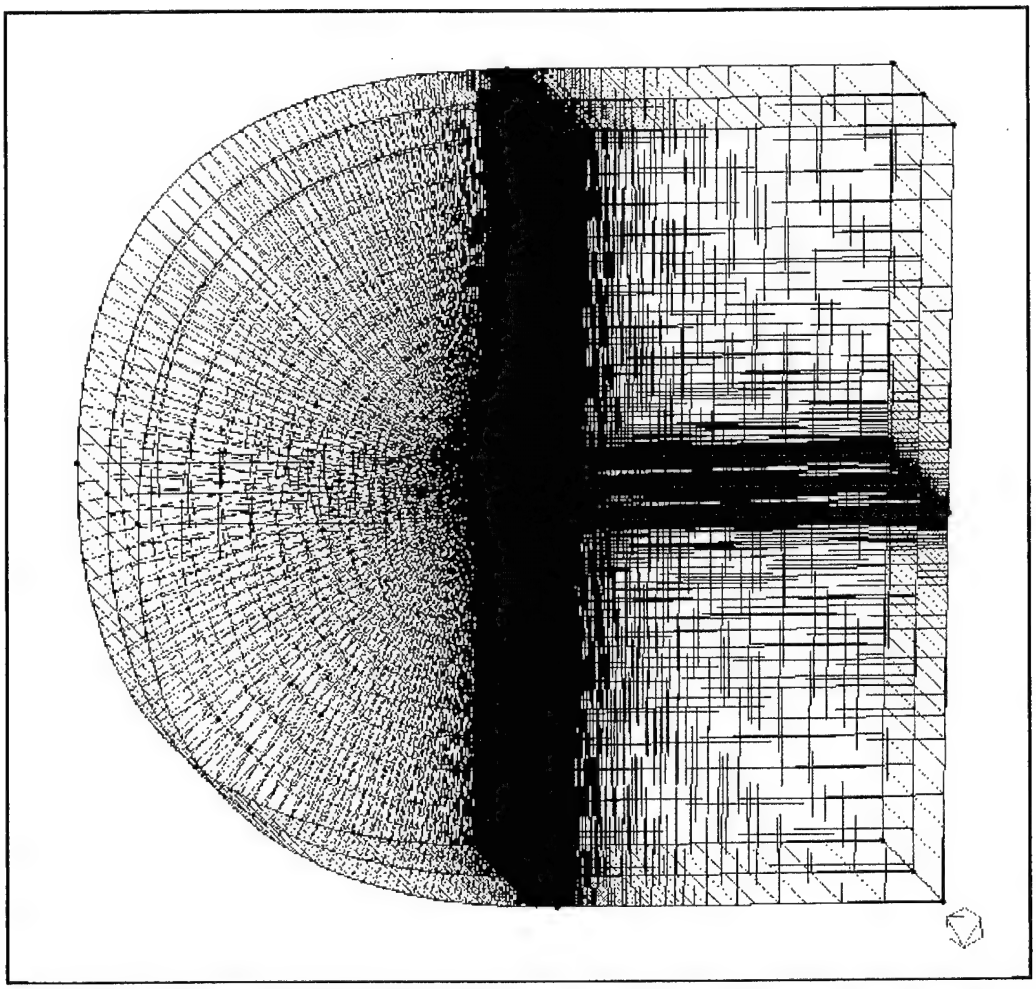

Figure 2.3 - Example of a GRIDGEN generated Three-dimensional Block Grid About a sail section.

5. Satisfactory grids (domains or blocks) are saved in PLOT3D/ASCII format to be used by the respective flow solver. For domain grids, a grid editing program (GRIDED) is used to edit the grids into true two-dimensional grids (GRIDGEN saves them in 3-D coordinates). GRIDED can also be used to adjust the grid index directions for proper configuration based on the flow solver to be used.

Since the majority of the OVERFLOW work was completed on the school's CRAY, a further step was required for the three-dimensional grids. Using another FORTRAN program the grid points were saved as an unformatted file, that also switched the 'y' and 'z' coordinates to coincide with the OVERFLOW file format. Each grid was subjected to another routine that reformatted the unformatted grid point file for a graphical inspection. These PLOT3D formatted grid files were viewed using the flow visualization program FAST [Ref. 17], and/or PLOT3D [Ref. 18].

The four shapes used for this report (Figure 2.4) were created from the same basic sail profile, but differ greatly in their look and composition. The first shape is a model of current windsurfer sails. The second shape only differs from the first in that it uses an elliptical leading edge vice the circular one of the original sail. The third and fourth shapes created, represent a proposed semi-rigid wing-sail that utilizes a rib made from a symmetrical airfoil (in this case a NACA 0012) at the front of the batten.

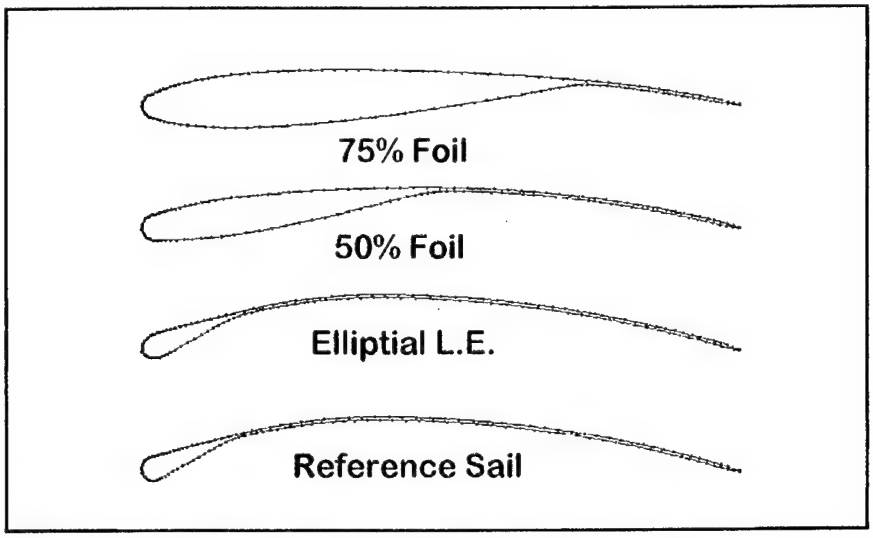

Figure 2.4 - Comparison of the Four Sail Shapes Analyzed

1. Standard Sail Model

To ensure this analysis was comparable to previous results, the initial sail model used came from Avila's work [Ref. 7]. Although this was not the primary model analyzed within that work, research into current windsurfer sails (see Figure 2.5) showed that it

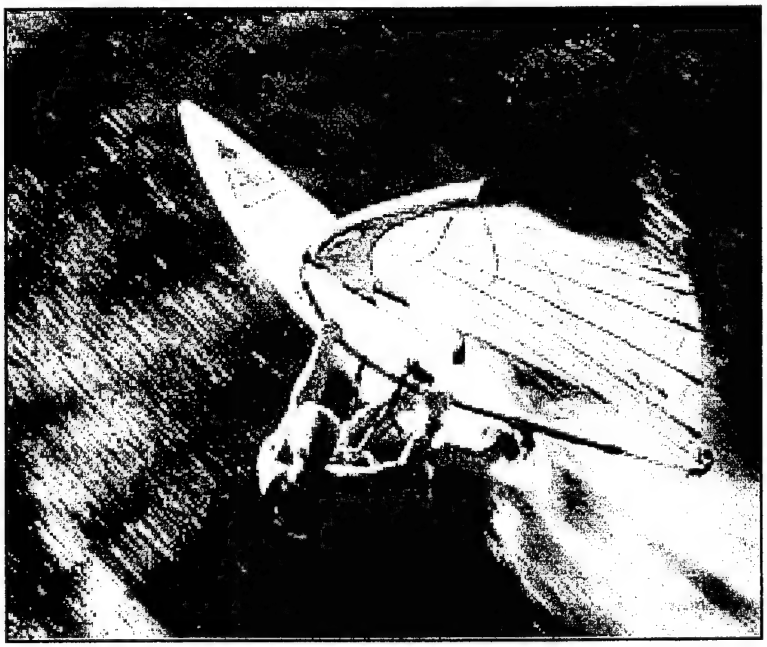

Figure 2.5 - Example of Current Windsurfer Sail in operation (note camber position and amount).

was more representative of actual sails under operating conditions. This shape consists of a circular mast section (2 % nominal value), an upper and lower straight line segment that represents the mast pocket, and the cambered (8.5%) membrane section that was generated with a second order polynomial forward of the maximum camber point (approximately 41% chord), and a circular arc for the aft portion. The original shape consisted of seventy-five upper and lower points, for a total of 150 (Figure 2.6).

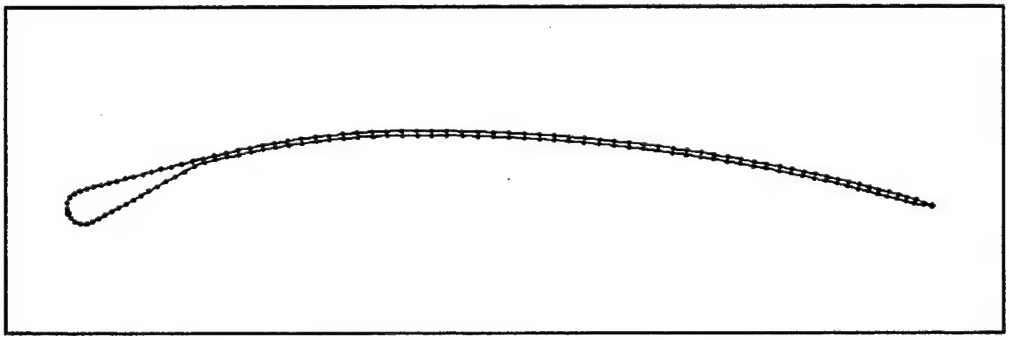

Figure 2.6 - Original Sail Gridpoints [Ref. 7].

This original shape was read into GRIDGEN as a gridpoint file where grid boundaries were added ten chord lengths away from the surface in a 'C' grid configuration. In its final version two hundred and eleven gridpoints were placed along the surface and seventy along the 'C' cut for a total of three hundred and forty-nine. One hundred grid points were added radially out from the sail to the grid boundary, with spacing starting at .0001 chord length at the surface. The surface gridpoints were distributed for finer resolution at the leading and trailing edges as well as the lower area of the mast pocket/sail interface. In creating the final grid, the original shape was altered

very little; smoothing was accomplished at the sharp trailing edge and the lower mast pocket sail interface, as well as at the circular leading edge (Figure 2.7).

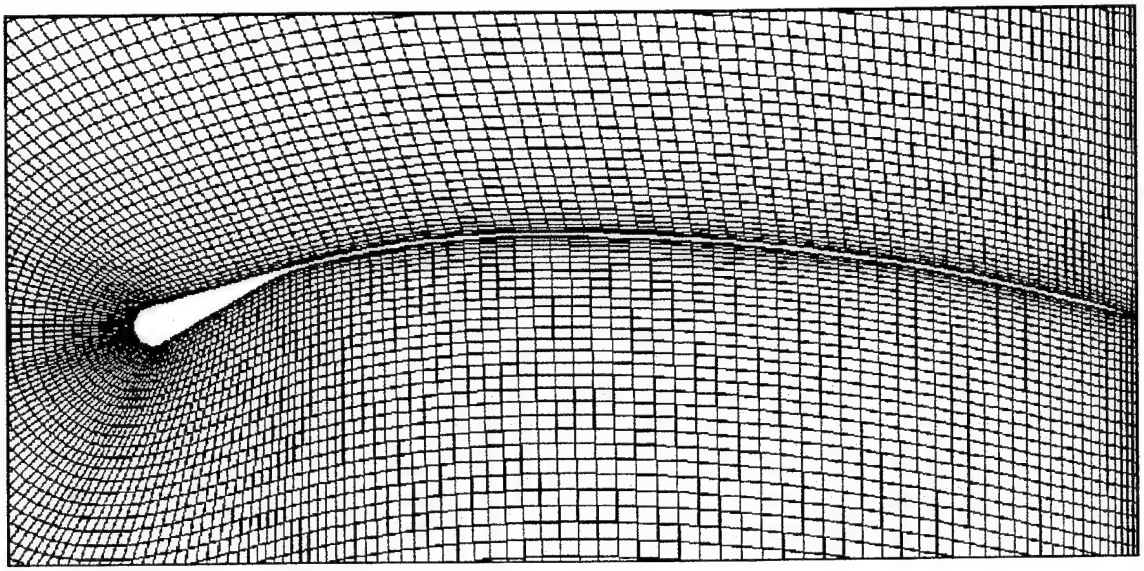

Figure 2.7 - Final Sail Grid.

2. Sail with Elliptical Leading Edge

In an effort to ease the rapid acceleration of the flow around the relatively large circular leading edge, and produce a more aerodynamic shape, an elliptical section of the same width as the original leading edge was inserted at the mast position. The straight segments representing the mast pocket were redrawn to fair the new forward portion but the original aft portion of the sail shape was not altered. Again the same number of grid points were defined throughout to alleviate compiling more than one reformatting code, and the same basic guidelines were followed in the distribution of the points about the surface. The main difficulty in generating the new shape was drawing and aligning the elliptical section using the limited tools within GRIDGEN (Figure 2.8).

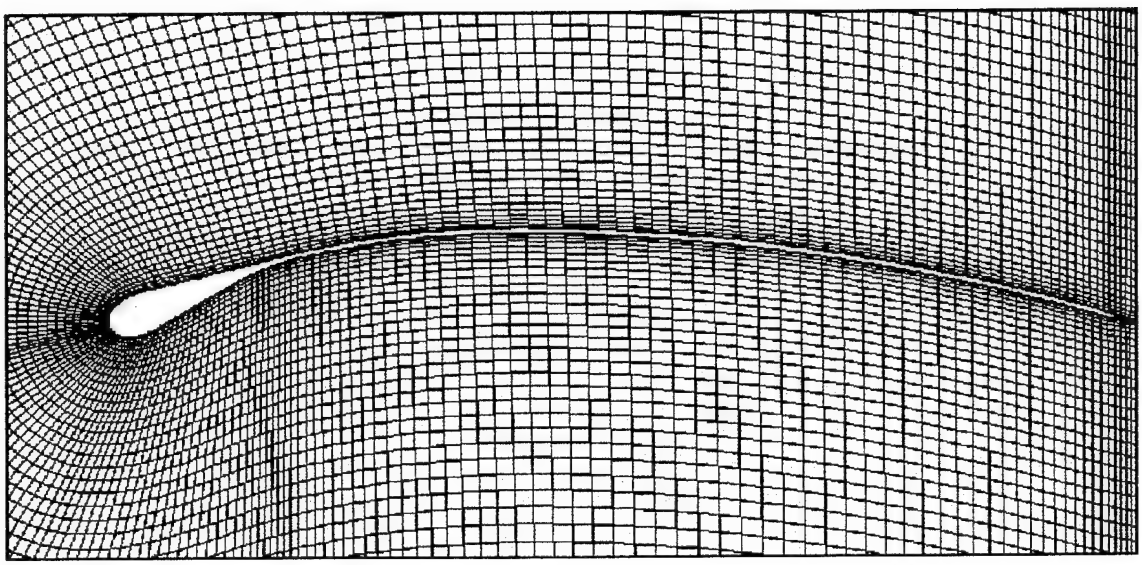

Figure 2.8 - The Elliptical Leading Edge Sail Grid.

3. Wing-sail with 50% Chord Symmetrical Foil Section

The original thought was to insert a NACA 0012 airfoil section equal to twenty-five percent of the sail chord length immediately following the leading edge mast section. In theory this would increase the relative suction on the upper surface while reducing flow problems at the mast pocket interface point. When attempted it was found that this length of foil section yielded a relatively small thickness that could not be readily faired to the circular leading edge. Although the leading edge of a NACA 0012 section that was fifty percent of the sail chord length was still much smaller than the mast radius, fairing the two shapes proved satisfactory. Within GRIDGEN the NACA 0012 section was collocated with the leading edge of the original sail shape and was rotated to a proper angle around the leading edge point. Simultaneously the aft section of the sail shape was rotated about the trailing edge point until the upper surface of the two shapes were

tangent at approximately the fifty percent chord point. The three shapes were split apart, removing the extraneous sections, and then joined together, ensuring smooth transition points at these new joints (Figure 2.9). The resulting shape's maximum camber point and the amount of camber was shifted somewhat (approximately 6.7% at the 47% point), while retaining the circular leading edge. As in the two previous grids the number of gridpoints and the placement was kept as standard as possible.

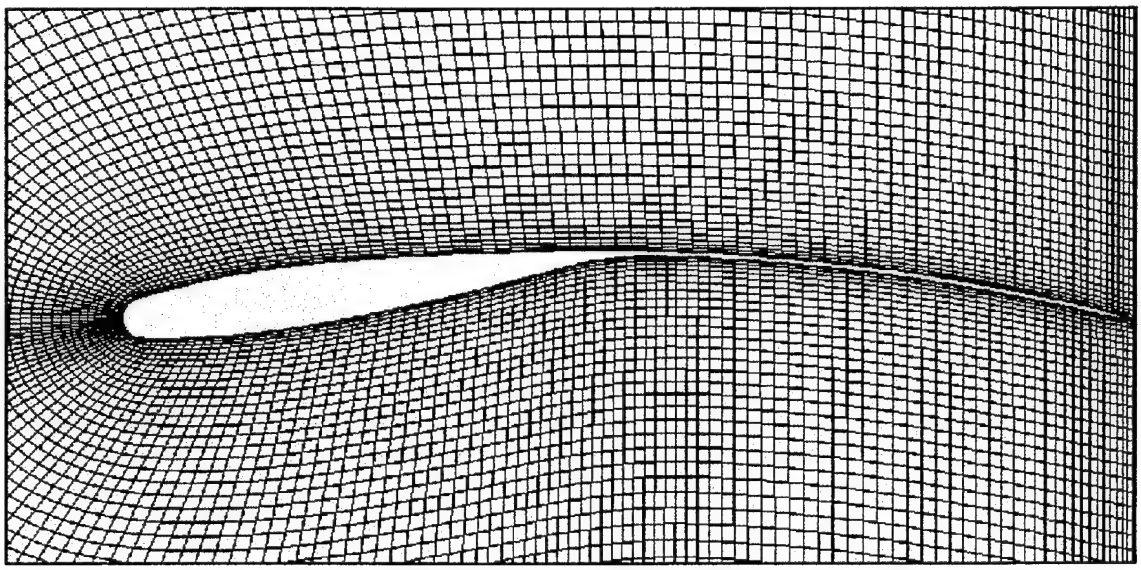

Figure 2.9 - Wing-sail Grid with 50% chord NACA 0012 section.

4. Wing-sail with 75% Chord Symmetrical Foil Section

It was thought that a longer and thicker airfoil section would provide a smoother transition at the leading edge portion and at the transition to the aft sail section. Using a seventy-five percent chord length NACA 0012 section, the difference between the circular mast diameter and the airfoil leading edge was much less and provided for a smoother joining of the two shapes. Again the aft portion and the NACA 0012 section were both rotated about their endpoints until they matched up, resulting in a shift of the

maximum camber position and amount (now approximately 34% and 6% respectively). The grid and grid point placement were almost exactly as in the first wing-sail grid (Figure 2.10).

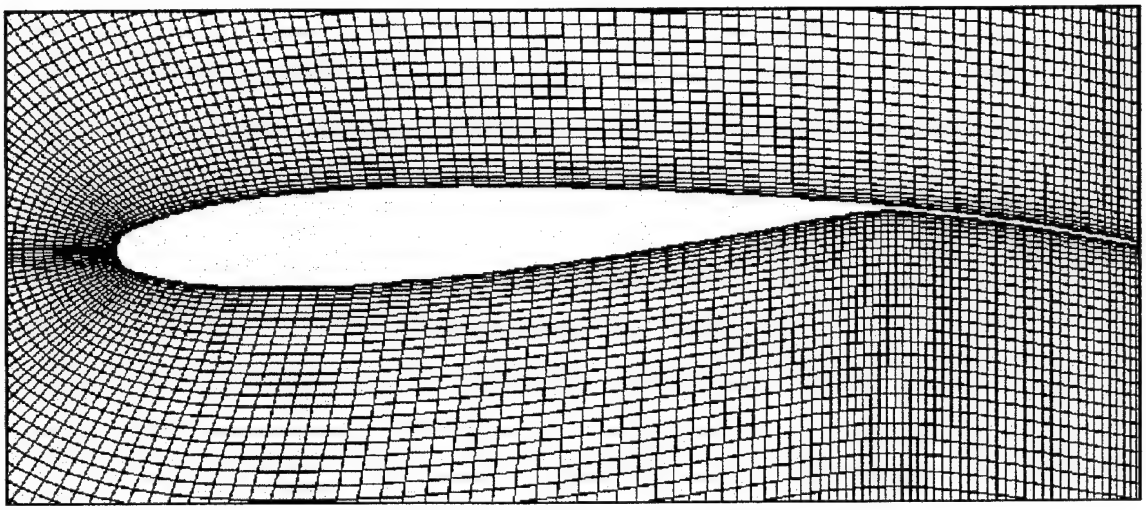

Figure 2.10 - Wing-sail Grid with 75% Chord NACA 0012 Section

5. Three-dimensional Wing-sail Model

The ultimate goal of this project is the demonstration of the feasibility of generating a three-dimensional sail model and the considerations required. This was not merely the placement of copies of the selected wing-sail section at intervals along a vertical mast. In fact several important steps were necessary to accurately model not only an actual wing-sail, but also how the flow interacts with a sail in its environment. The first step was to analyze how a typical sail is trimmed with respect to the shifting apparent wind as it moves through the atmospheric boundary layer. Using several photographs of sails in operating conditions, the angle of attack of the sail as a function of height can be

approximated by the chord lines drawn from the mast leading edge to the batten ends (Figure 2.11). Using these measurements and the true wind velocity profiles presented in chapter one, the proper incident angles for each sail section can be calculated (calculated positions of each wing-sail section are presented in Appendix D). Making the shape even

Figure 2.11 - Illustration of Sail Twist Angle Approximations.

more difficult to construct is that while it is fairly easy to scale the chosen sail section for the desired lengths necessary for each segment, the mast tapers from its base to its tip. For this reason nearly half of the 10 chosen sections used to construct the three-dimensional model had to be altered in GRIDGEN prior to being added. For each section, a scaled version of the two-dimensional wing-sail section is read into GRIDGEN, combined with the proper mast radius leading edge, and then the whole profile is rotated to its calculated setting angle. After each section is properly scaled and rotated, they can be read into GRIDGEN to be combined with a vertical mast line that follows the path of a

standard windsurfer sail mast. Finally after stacking the wing-sail's sections at their predetermined heights, far-field grid boundaries for each section must be placed at these same heights. Domains at each level are made from these and then the whole system must be blocked together (Figure 2.12). A stinger-like segment must be used at the masthead while the base of the mast can pierce what will be a shear wall. Another method to accurately model the flow would entail defining the atmospheric flowfield as an input to the flow solver.

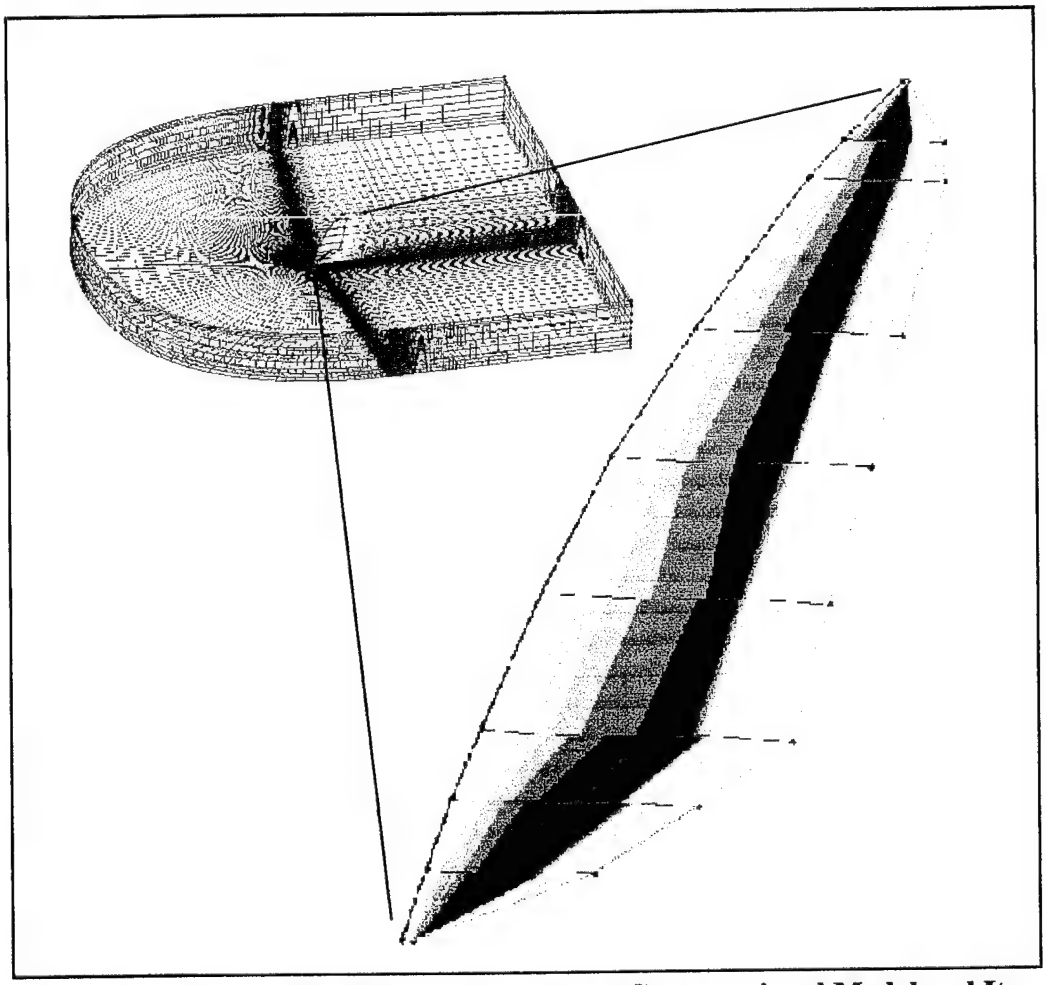

Figure 2.12 - Image of the Three-dimensional Computational Model and Its Associated Grid.

III. COMPARATIVE RESULTS

As described in the previous chapter, a CFD analysis is inherently iterative, and good and timely results are arrived at by an almost intrinsic ability to make decisions on input parameters and grid changes. This is what many deem "the Art of CFD" [Ref. 13]. This ability to make the right decisions is only developed through a thorough understanding of the code used and extensive experience in this field (i.e. learning the hard way what works and what doesn't). Due to time limitations not all configurations could be fully analyzed (adequate results for the three-dimensional wing-sail model could not be produced). Each of the two codes reacted differently to changes in the input parameters, and with eight different solutions being developed almost simultaneously, tracking the modifications and different results became a task of file management.

There are many ways to view and compare the results of the CFD analyses performed here. Two available programs that can read the resulting '*Q*' files, calculate the flow description quantities (velocity, density, pressure, etc.), and display the flowfields respective to those quantities, are PLOT3D and FAST. PLOT3D is the standard for file format, and its ease of use makes it ideal for quick evaluation and comparison of results. On the other hand FAST allows for more flexibility in viewing and displaying the resulting flowfields, and also offers additional tools not available PLOT3D [Ref.s 16 and 17]. In this chapter the flowfields are displayed using FAST while coefficient of pressure (C_P) distributions were plotted using a standard spreadsheet program.

Since the majority of the analysis is two-dimensional, comparisons between OVERFLOW and the two-dimensional Navier-Stokes (referred to as NS here) were made

at different angles-of-attack (AOA) using the original sail shape, and the same flow parameters, in order to validate the OVERFLOW results. A comparison of the flowfields at each AOA was made between the two different codes, and Avila's previous results [Ref. 7]. Additionally the calculated C_P distributions from OVERFLOW were plotted against those produced from NS (Figure 3.1).This showed reasonable agreement between the two codes and the previous work, and since the analysis would be comparitive using the same code and methods, the technique was deemed to be valid.

All analyses were made at a freestream Mach number of 0.2, a Reynolds number of 800,000, and standard day tempurature. (Note: C_P distribution plots show the values reversed for standard display purposes)

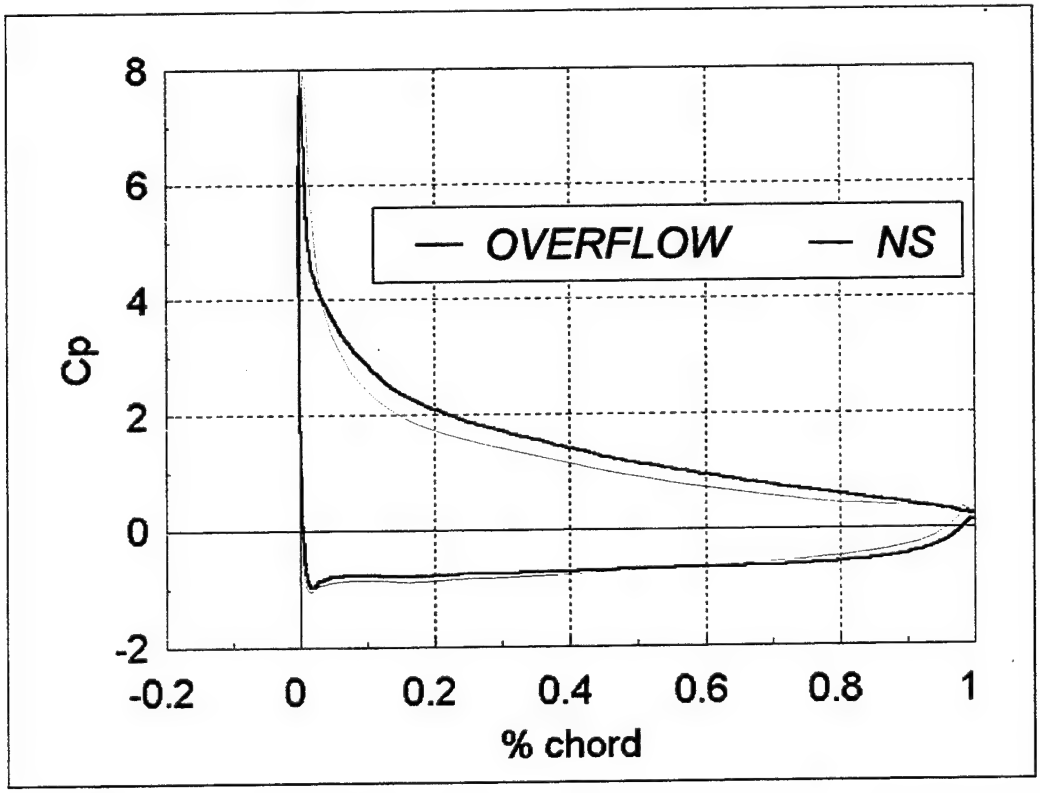

Figure 3.1 - Example of Coefficient of Pressure Distribution Comparison Between OVERFLOW and NS for the Reference Sail Shape at 14° AOA.

A. VELOCITY VECTORS

Overall the behavior of the velocity vectors were very similar across the different surfaces. The shapes that used the circular mast leading edge, such as the original sail shape were prone to flow reversal on the upper surface just after the transition to the mast pocket. While at moderate AOAs the flow reattached to the surface, it did cause the flow to slow rapidly towards the trailing edge on the upper surface, which in turn produced flow reversal here as well (Figure 3.2). Plots of the velocity vectors for the four

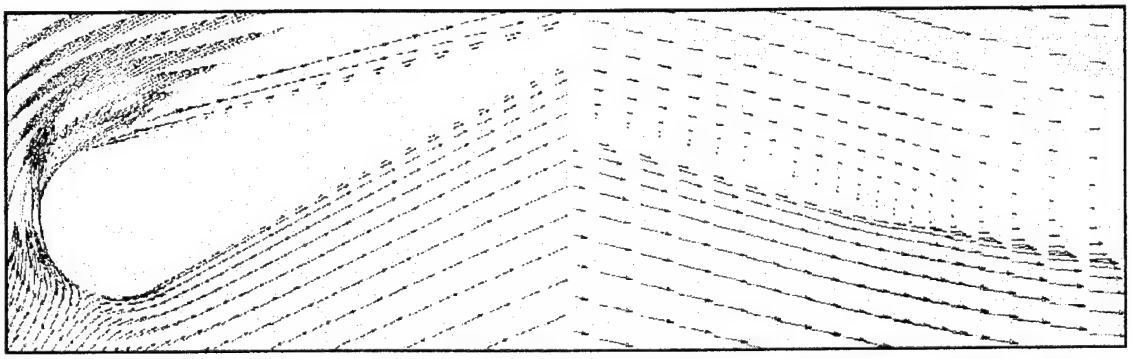

Figure 3.2 - Velocity Vectors at Leading and Trailing Edges of Windsurfer Sail.

shapes at a moderate AOA are presented on the following pages to illustrate their behavior (Figures 3.3 - 3.6). It is of note that lower AOAs were not attempted because the flow would not realistically generate the pressure differential to maintain the desired camber. At angles causing separation at the lower surface mast pocket/ sail transition point the membrane of the sail would collapse and begin to flutter.

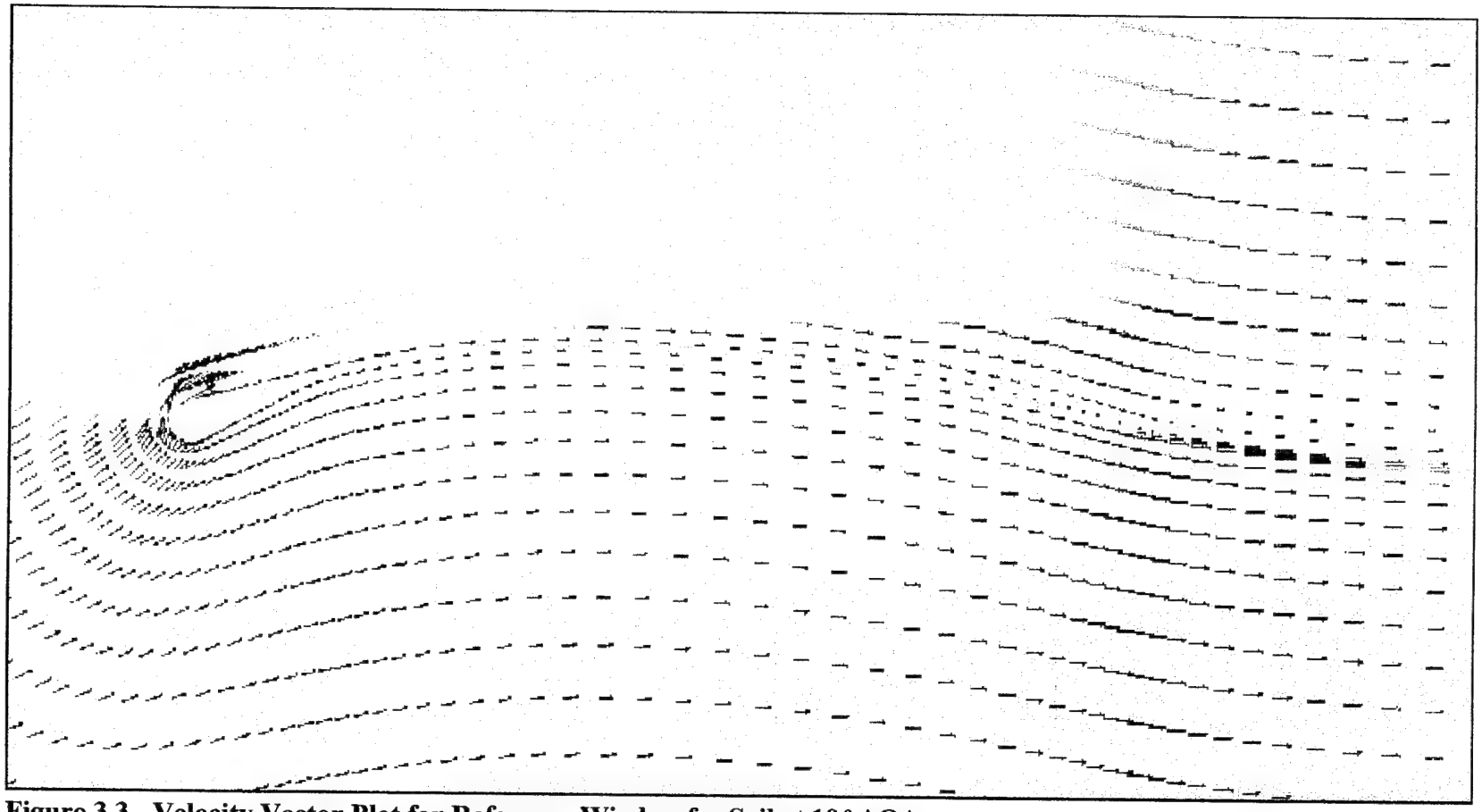

Figure 3.3 - Velocity Vector Plot for Reference Windsurfer Sail at 10° AOA.

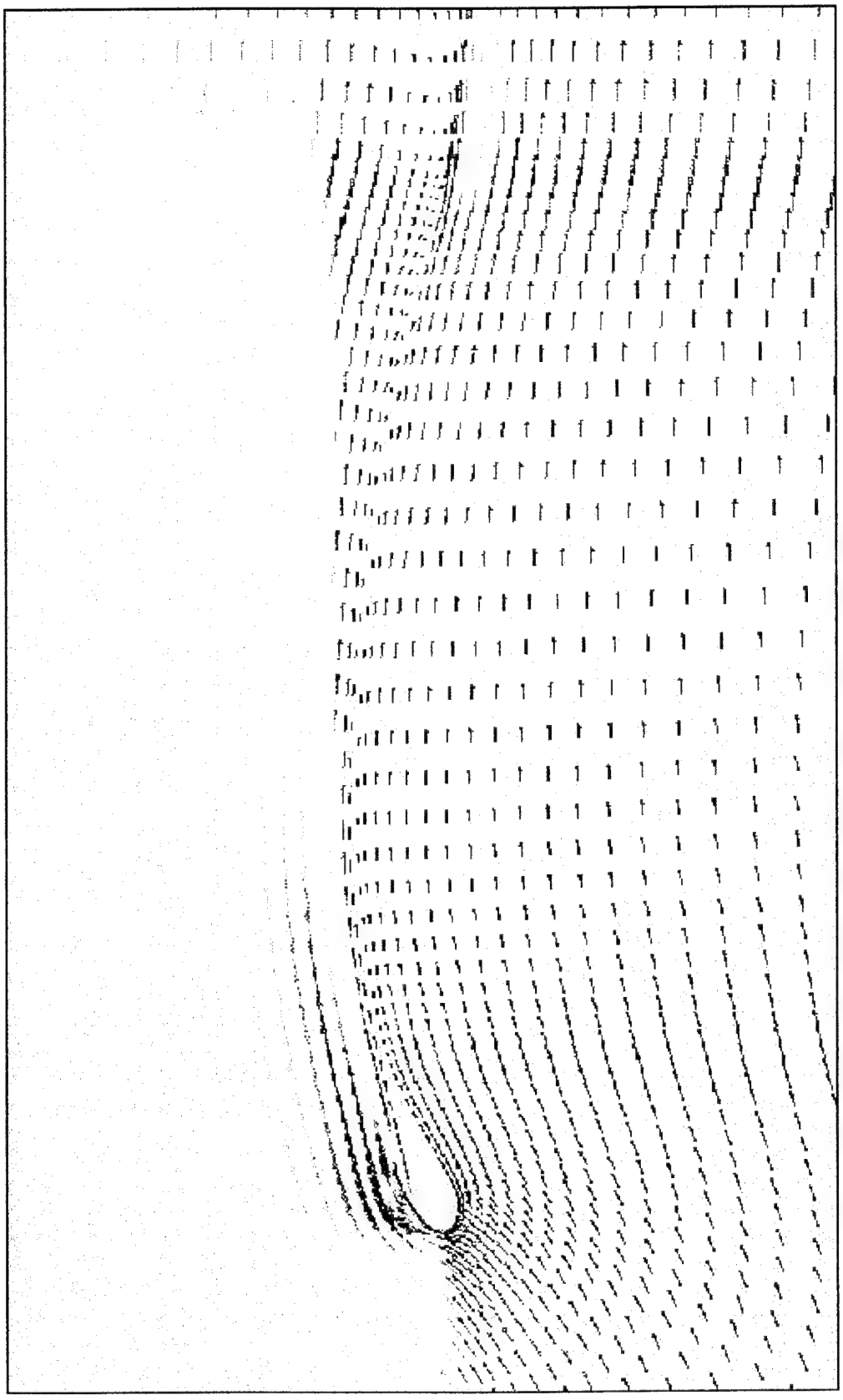

Figure 3.4 - Velocity Vector Plot for Elliptical Leading Edge Sail at 10° AOA.

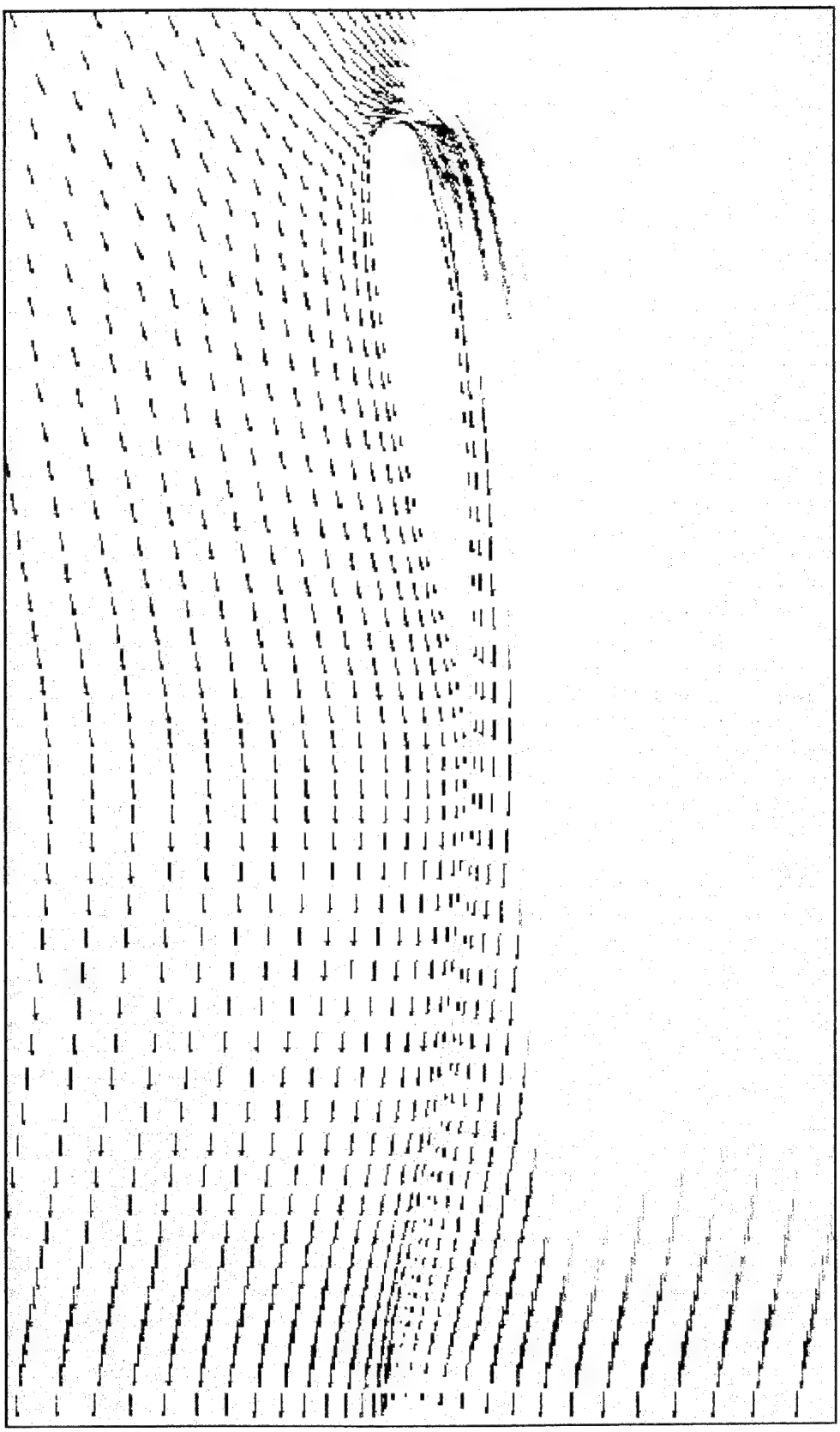

Figure 3.5 - Velocity Vector Plot for 50% Symmetrical Foil Wing-Sail at 10° AOA.

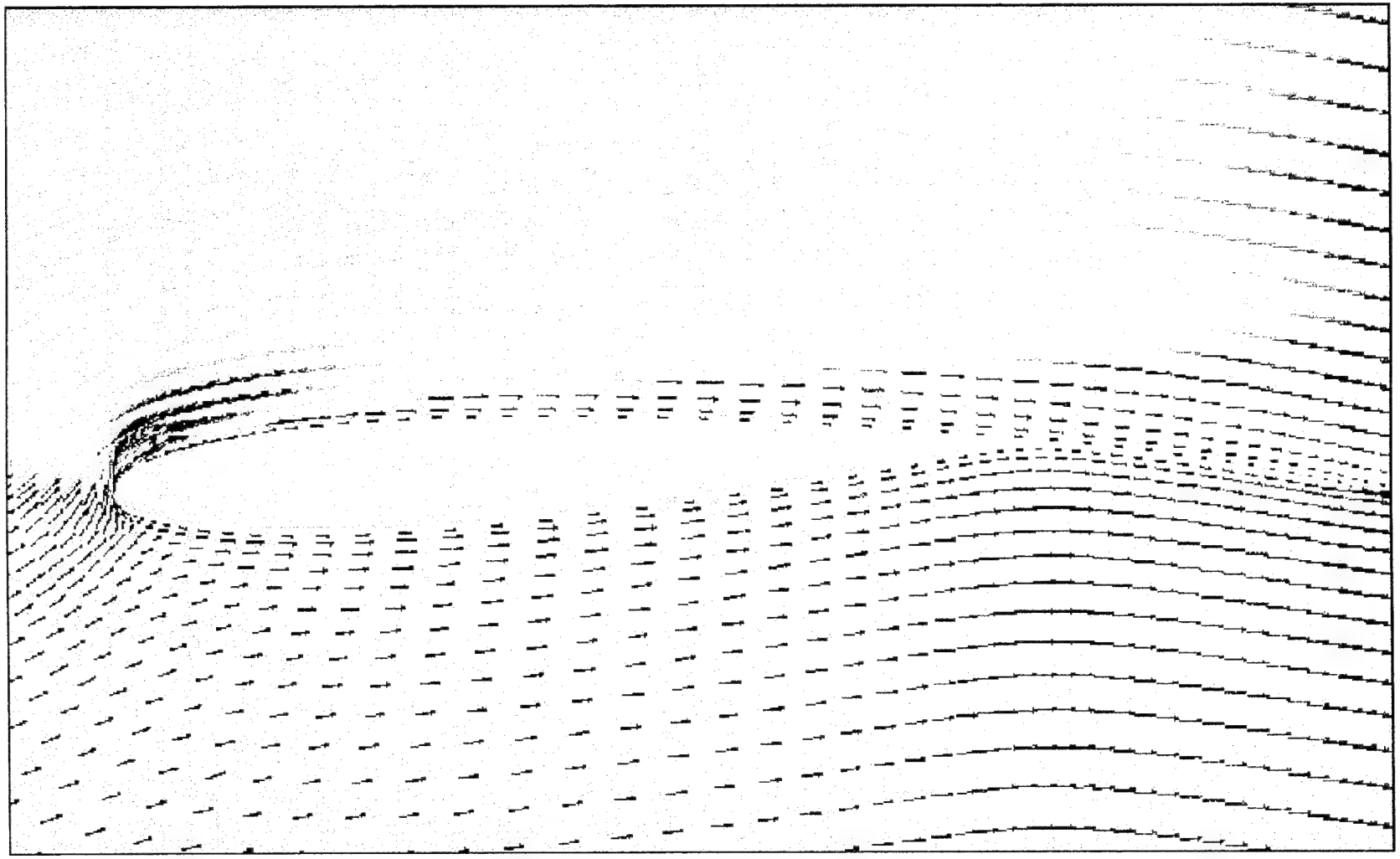

Figure 3.6- Velocity Vector Plot for 75% symmetrical Foil Wing-sail at 10° AOA.

B. PRESSURE CONTOURS

Pressure contours show more clearly the difference in the flows about the four shapes. Below (Figure 3.7) a close-up of the leading edge of the windsurfer sail shows how the contours delineate the area of maximum and minimum pressure. The fact that both are located so far forward on the sail illustrates the inefficiency of the overall

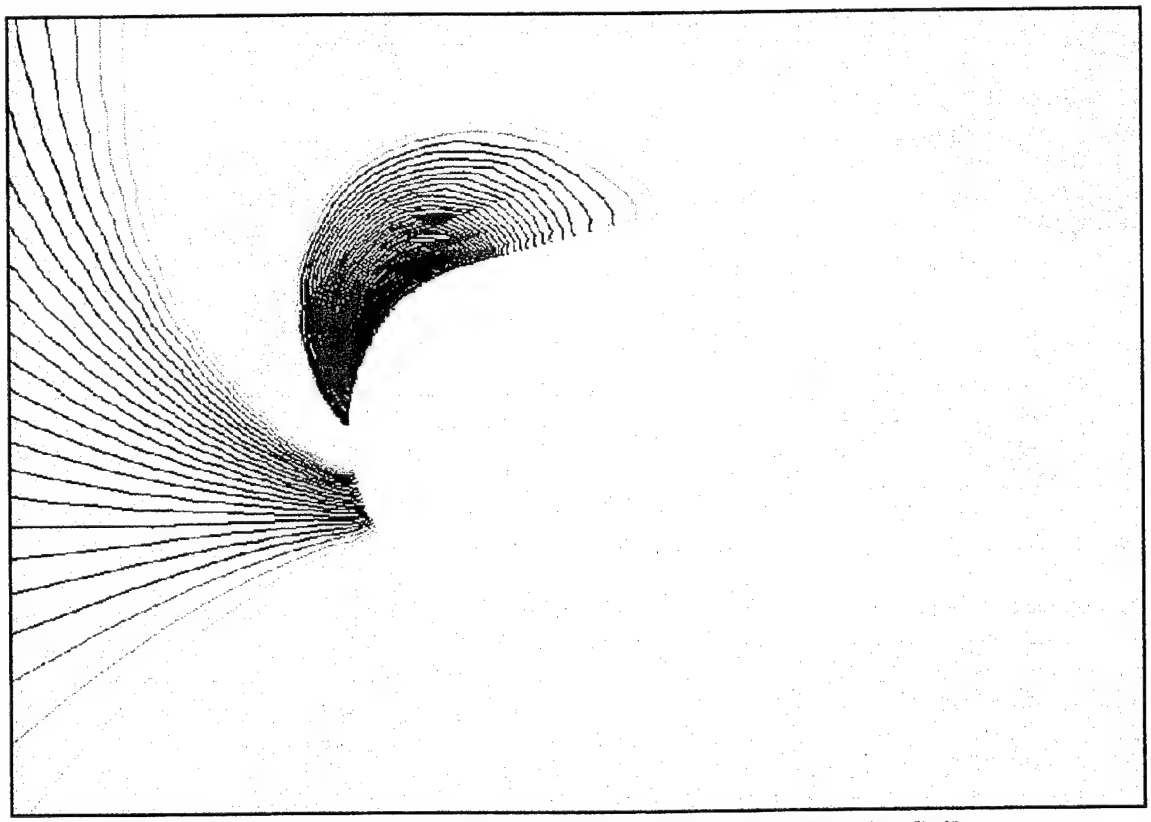

Figure 3.7 - Pressure Contours at the Leading Edge of Windsurfer Sail.

design when compared to modern airfoils. Plots of the pressure contours for the four shapes at a moderate AOA are presented on the following pages to illustrate their behavior (Figures 3.8 - 3.11).

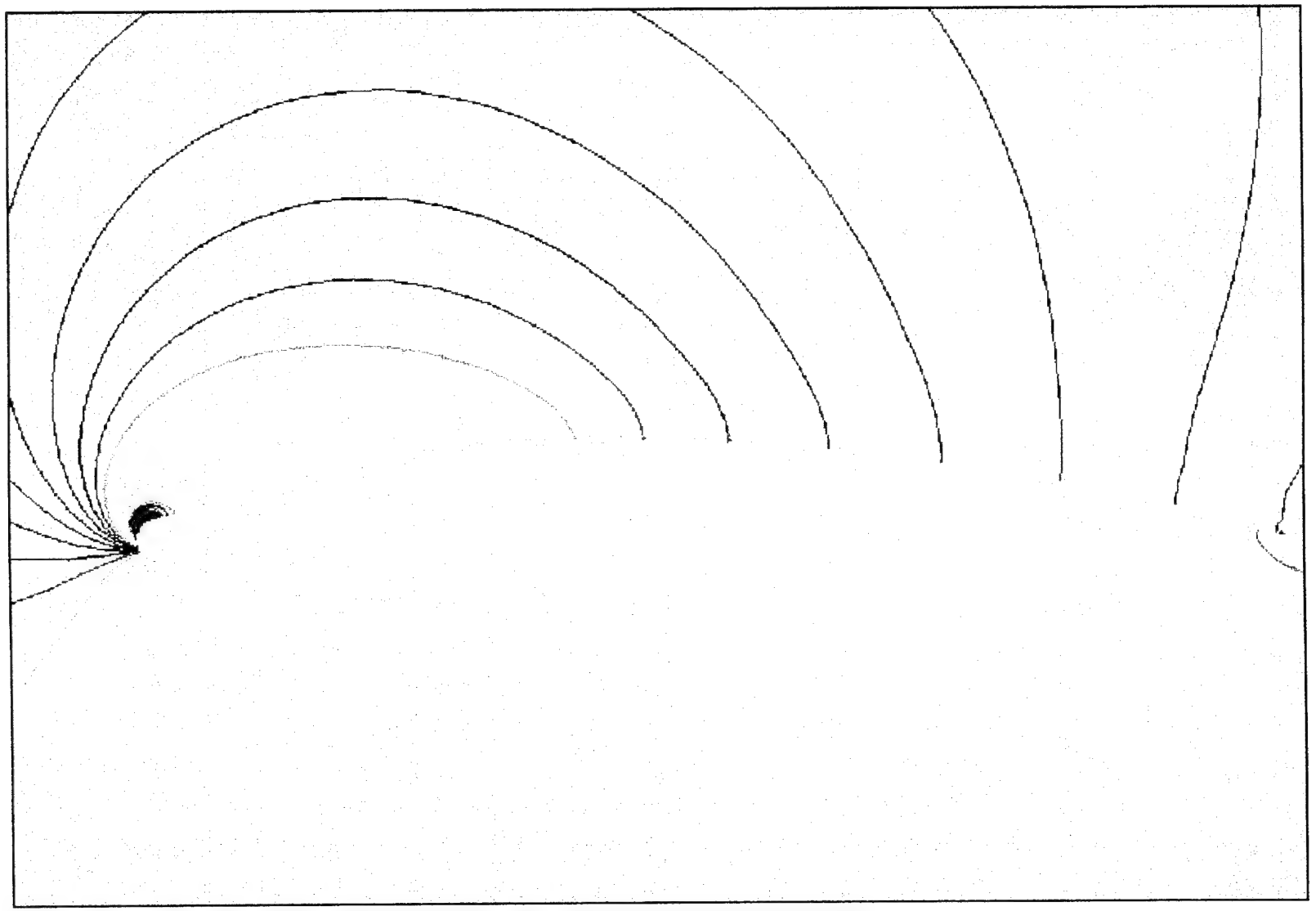

Figure 3.8 - Pressure Contour Plot for Reference Windsurfer Sail at 10° AOA.

Figure 3.9 - Pressure Contour Plot for Elliptical Leading Edge Sail at 10° AOA.

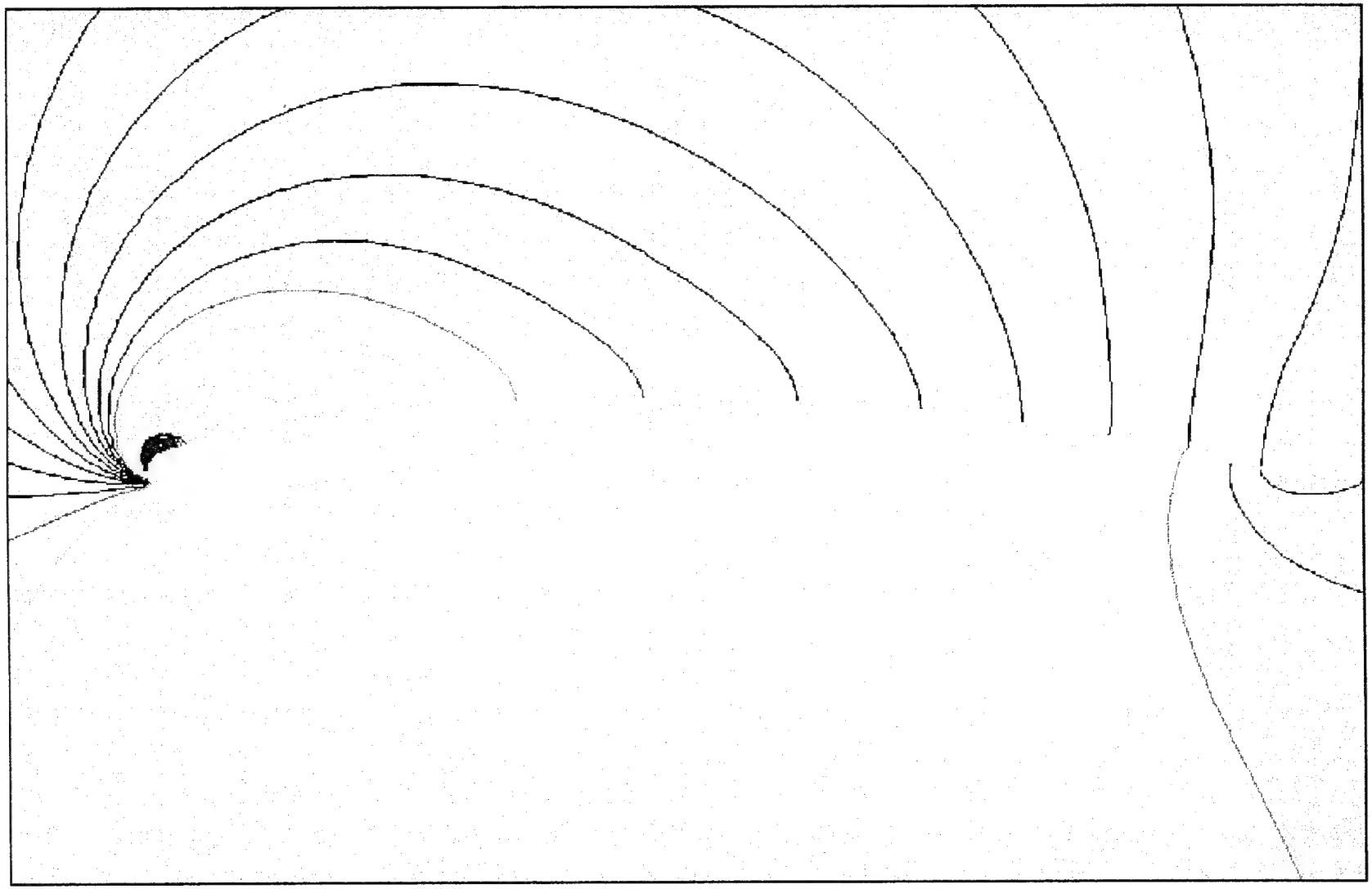

Figure 3.10 - Pressure Contour Plot for 50% Symmetrical Foil Wing-sail at 10° AOA.

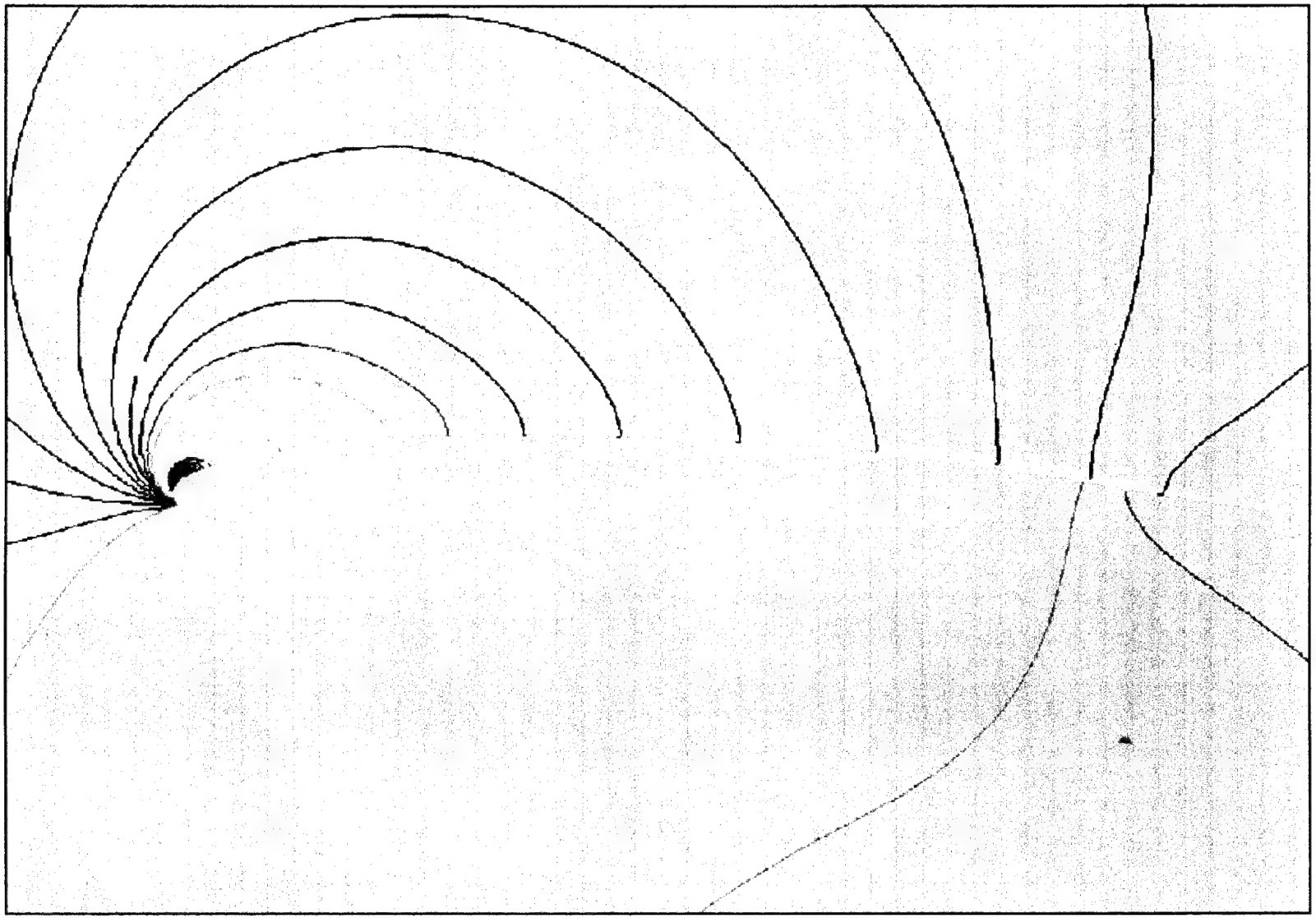

Figure 3.11 - Pressure Contour Plot for 75% Symmetrical Foil Wing-Sail at 10° AOA.

C. PRESSURE DISTRIBUTIONS

The easiest method of comparison and the one that more clearly demonstrates performance differences between the different shapes is a C_p distribution plot. By plotting the C_p distribution from each shape over a range of designated conditions, a performance trend can be established. As is demonstrated in the following plots (Figures 3.12 - 3.14), the original sail shape suffers from an extremely high and concentrated

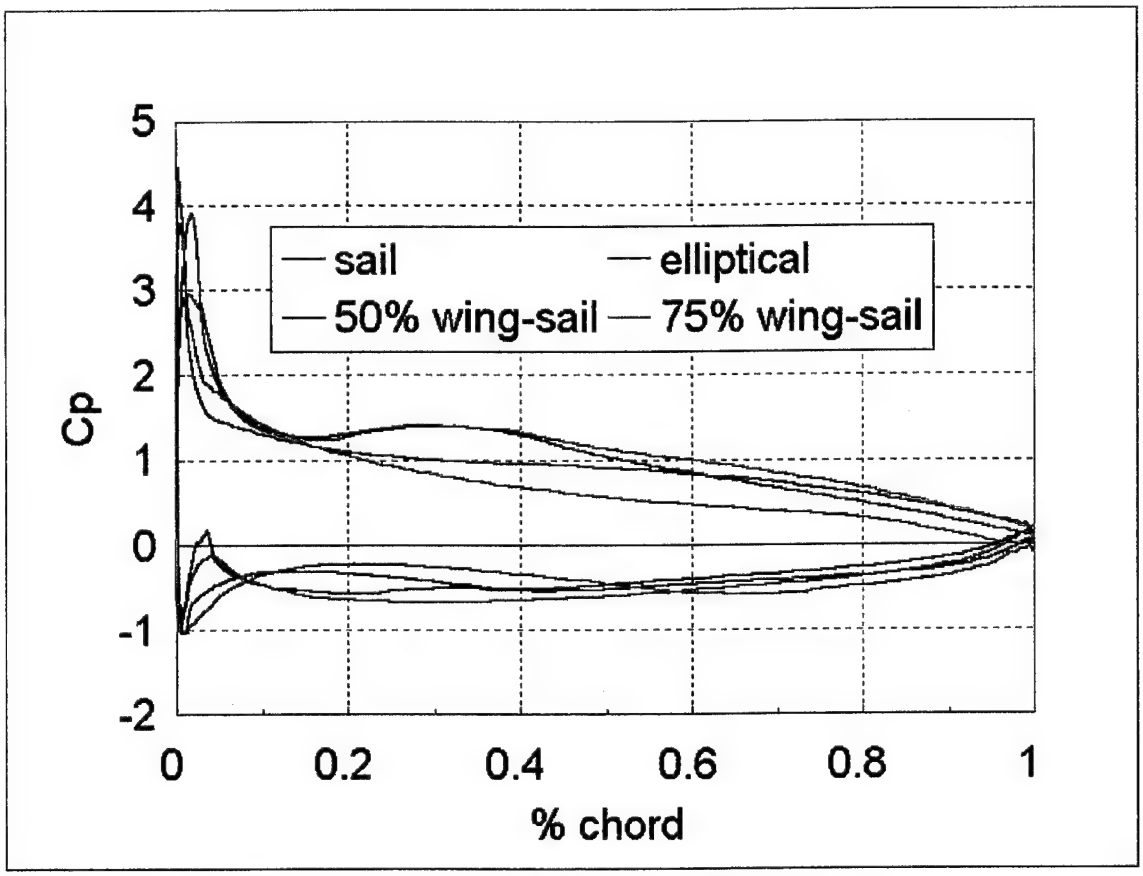

Figure 3.12 - Coefficient of Pressure Distribution Comparison, 6°

pressure gradient on the upper leading edge. This results in two very significant deterrents to performance. Since the area of highest pressure is collocated with that portion of the shape with the highest surface gradient orthogonal to the freestream flow

direction, the resulting drag is high. This extreme pressure gradient also contributes to the tendency of the flow to reverse and separate, resulting in vortex shedding at higher AOAs (this also makes a steady-state solution at high AOAs nearly impossible to produce).

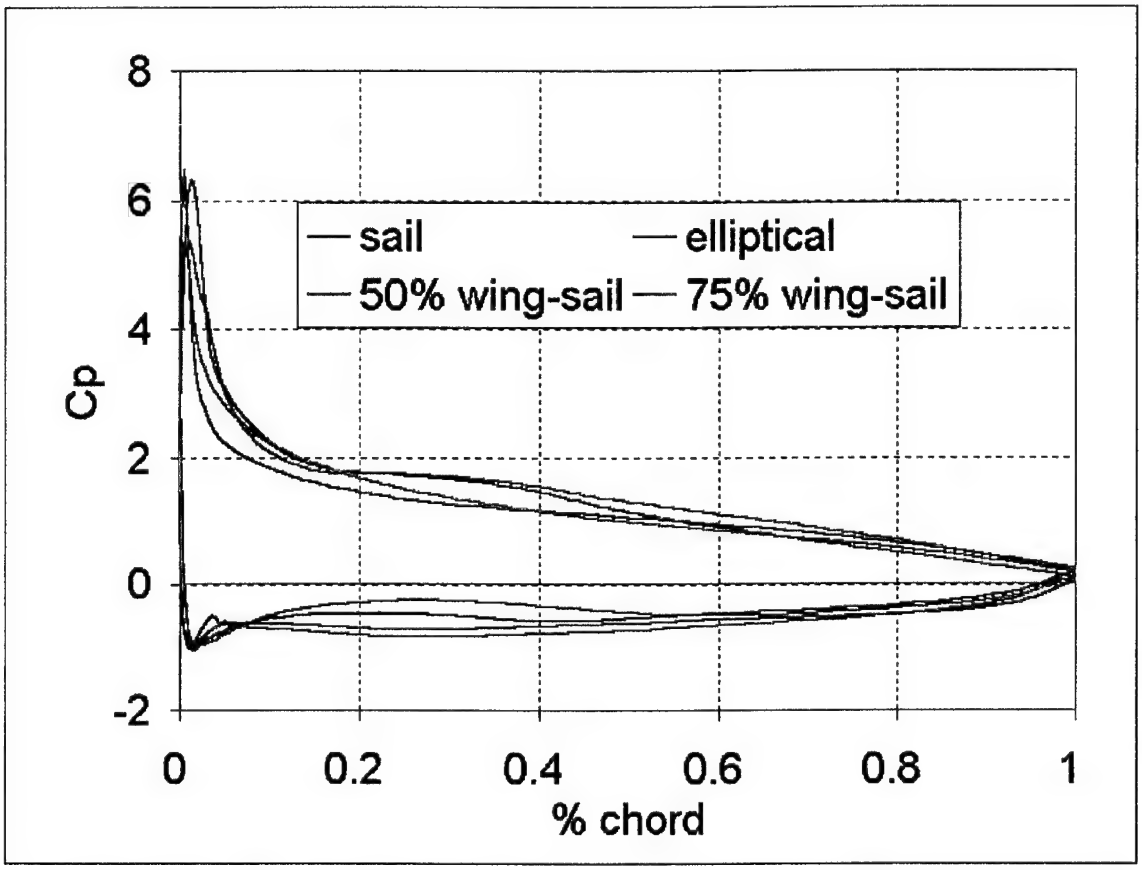

Figure 3.13 - Coefficient of Pressure Distribution Comparison, 10°

The most surprising feature of these plots is the performance of the elliptical leading edge sail with respect to the wing-sails, especially at low AOA. At lower AOA the additional thickness of the wing-sails actually work against them in that the flow across the lower surface must also accelerate (reducing lift). While this is visible on all

the configurations it affects the wing-sails greater relative to the length of the foil inserts and the reduced effective AOA on the front portion. At higher AOA the elliptical leading edge sail continues to outperform the 50% wing-sail. The fact that these two shapes produced nearly the same performance improvements by such differing methods was unexpected. As is visible in the plots, both shapes produce a lower peak pressure

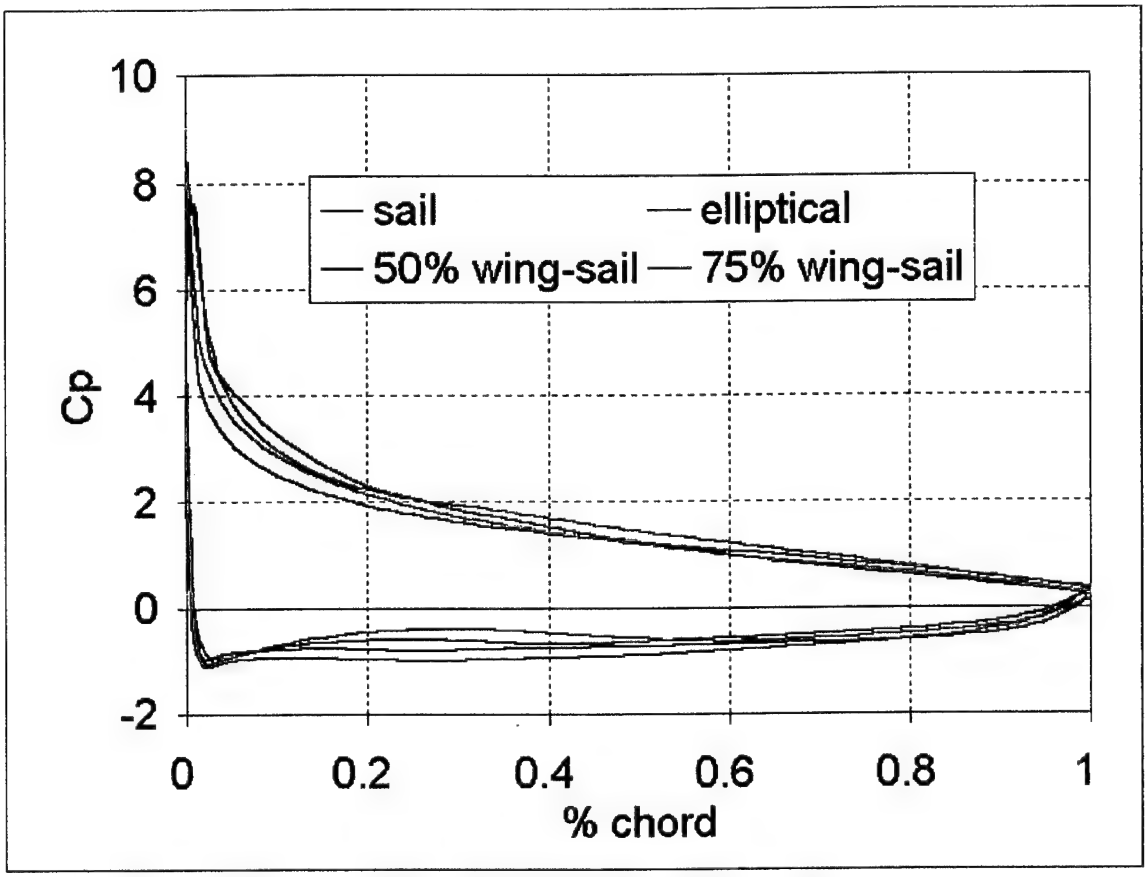

Figure 3.14 - Coefficient of Pressure Distribution Comparison, 14°

difference at the leading edge while providing for greater pressure difference (hence greater lift) on the aft portions. To get a better representation of how the pressure changes with change in AOA, a plot of the C_P distributions for the elliptical leading edge sail for a range of AOA was made (Figure 3.15). The difference in pressure between the

upper and lower surface increase, indicating an increase in lift, with a corresponding increase in AOA, as expected. It is also observed that a bump that forms in the distribution on the forward part of the upper surface corresponds to the formation of a separation bubble at 16° AOA, which gets significantly larger at 18° AOA.

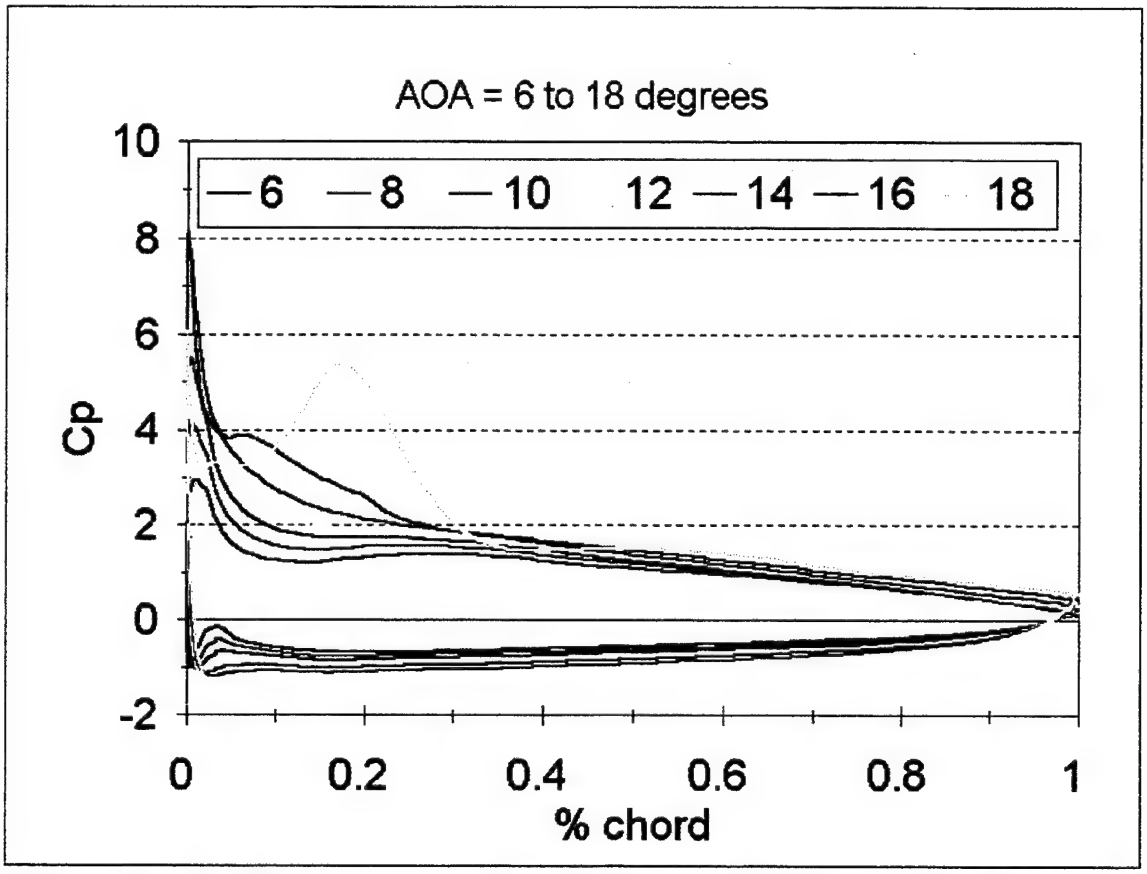

Figure 3.15 - Coefficient of Pressure Distributions for Elliptical Leading Edge Sail

D. STALL CHARACTERISTICS

Stall characteristics are inherently hard to ascertain using CFD analysis, since the goal of such analysis is to approximate the steady state solution, and stall is a naturally unsteady phenomenon. While it is extremely difficult to determine if a stalled condition produced by this analysis is in fact physical or realistic, how the flowfield develops while

the solution proceeds is enlightening. In the case of the original sail shape, vortices are produced aft of the leading edge and after growing to a significant size begin to shed and travel with the flow to the upper right of the grid. Not long afterwards vortices begin to form and shed from the trailing edge (Figure 3.16). To compare this with empirical data,

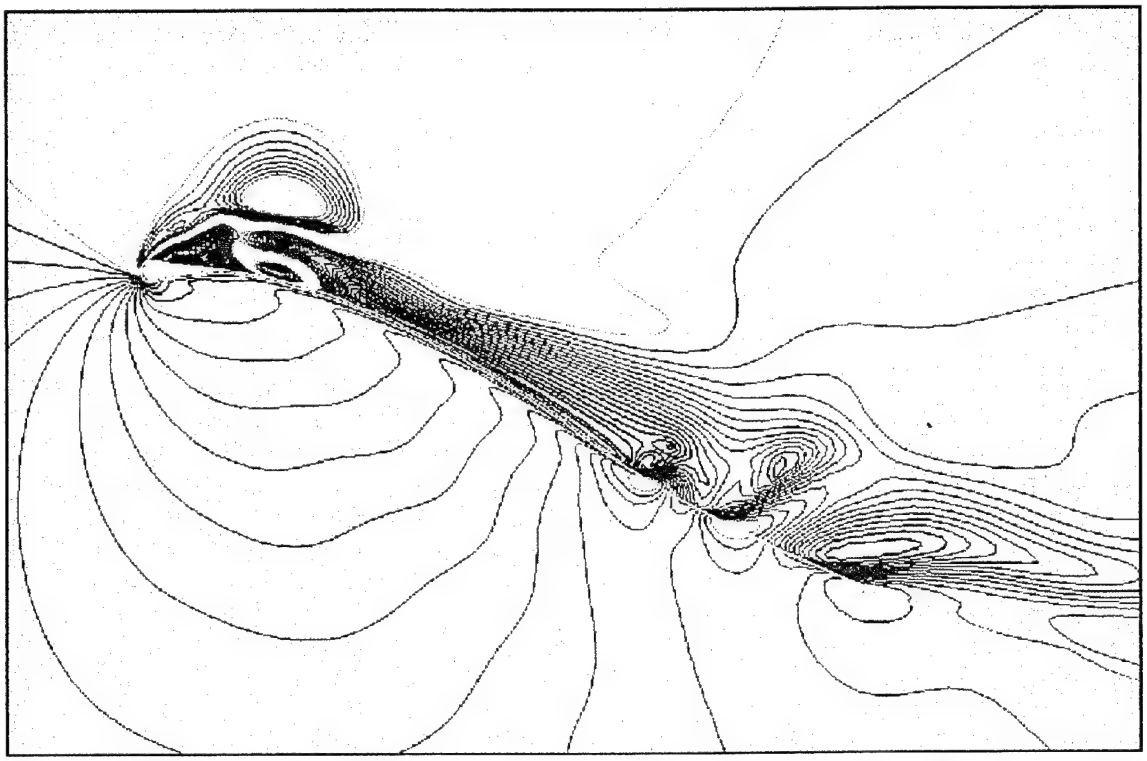

Figure 3.16 - Contours of Velocity magnatudes Illustrating Shedding Vortices on Reference Windsurfer Sail at 18° AOA.

photographs of traditional sailboat sail shape undergoing wind tunnel tests were found on the Internet in Finland (Figure 3.17). The below photo is an enhanced version of a smoke test done in the low speed wind tunnel at the University of Helsinki. Although the leading edge/mast section is quite different, it demonstrates the same general behavior of the flow at stall, as seen with the OVERFLOW results.

Figure 3.17 - Photograph of Sail Shape in a Stalled Condition During Wind Tunnel Tests, 27° AOA (University of Helsinki).

IV. CONCLUSIONS AND RECOMMENDATIONS

A. CONCLUSIONS OF ANALYSIS

It was believed that like the improvements modern thick airfoils have demonstrated over early thin shapes, the proposed semi-rigid wing-sail would provide a clear advantage over the original sail shape. Interestingly the results presented here demonstrate the leading edge shape has a more profound effect on performance than the foil thickness. At almost every point the elliptical leading edge sail showed improved lift, reduced drag and the ability to operate at higher AOAs. The primary reasons for the lackluster performance of the wing-sails are two-fold. First by retaining the circular mast leading edge, the wing-sails were consigned to suffer the same performance degradation seen with the original windsurfer sail. Second, increasing the thickness of the shape inadvertently decreased the effective camber of the wing-sail shape. In fact, as seen from the C_p plots, at lower AOA the thickness of the forward portion of the foil actually works against the overall performance when the flow is forced to travel nearly as far as the flow across the upper surface.

Overall the project clearly demonstrated that these techniques are viable methods of improving the performance of sails. The progress achievable by introducing these advanced scientific methods into an area of design that has traditionally been governed by seat-of-the-pants, and trial-and-error techniques, is limited only by the imagination and determination of those designers with the foresight to seize the future. Combined the latest in CAD/CAM tools, a sailmaker with the ability to accurately model fully viscous and turbulent flows will be able to produce sails that offer a significant improvement over

even the latest designs. Even the simple replacement of a traditional windsurfer sail, with one that has an elliptical insert at the front of the mast pocket should, according to these results, provide for a marked improvement in the ratio of Lift to Drag. Further refinements in sails and wing-sails from CFD analysis are only a matter of time. With the next America's Cup to be held in the spring of 2000 just around the corner, all sailors should expect the technology "trickle-down" to include CFD shaped sails.

B. RECOMMENDATIONS FOR FURTHER STUDY

The first and foremost recommendation is that others attempt and complete the final phase of this project by constructing and analyzing the flow about a three-dimensional sail model. The methods presented here should serve as satisfactory stepping stones for anyone who has access to similar equipment and technology for such a study. At the same time and although the CFD method has been validated as an analysis tool, backing-up a three-dimensional analysis with experimental results would go a long way to verifying CFD as a sail design tool.

Another recommendation comes from experience with the NS Fortran code. Although proven to be a valid and accurate method of analyzing two-dimensional flowfields, the code does require a significant amount of CPU time, especially when compared to the three-dimensional OVERFLOW code. Perhaps by utilizing a fourth-order Runge-Kutta scheme, already proven to significantly reduce computing time, the code may be made more efficient and become even easier to employ on available computer resources.

Finally, the last recommendation is for any sailors who read this report. The sailing community has long relied on tradition, and design methods proven through years of experience. The past two years have seen an increase in the amount of new technology applied to the sport. Faster boats, lighter and stronger equipment, and bigger sails are moving the baseline of recreational sailing to a new level. It's time the entire community embrace the methods and techniques established by the field of aviation. No other field of activity is as close to sailing as flying, yet sailors have consistently ignored the possible benefits available from flight mechanics. Yes there have been many inroads at the upper echelons of the sport, but with the technology and power available to every sailor with a home computer, the fruit of the techniques presented here should reach throughout the entire sailing community.

LIST OF REFERENCES

1. Donaldson, Sven, *A Sailor's Guide to Sails*, Dodd, Mead & Company, 1984.

2. Reichel, John, "Countdown to 2000," *Sailing World*, Vol. XXXV, No. 1, January, 1996, pp. 32-33.

3. Irey, Richard K., Hays, G. Murray, "The Effect of Onset Vorticity on Potential Flow Prediction of Sail Performance," *The Ancient Interface XVI: Proceedings of the Sixteenth AIAA/SNAME Symposium on the Aero/Hydronautics on Sailing*, Peter Lissaman, ed. Western Periodicals Co., 1986, pp. 22-28.

4. Lissaman, P.B.S., "Lift in a Sheared Flow," *The Ancient Interface XVI: Proceedings of the Sixteenth AIAA/SNAME Symposium on the Aero/Hydronautics on Sailing*, Peter Lissaman, ed. Western Periodicals Co., 1987, pp. 141-148.

5. Smith, R.W., "An Inviscid Analysis of the Flow About Windsurfing Sails," *The Ancient Interface XVII: Proceedings of the Seventeenth AIAA Symposium on the Aero/ Hydronautics on Sailing*, William Feiereisen, ed. Western Periodicals Co., 1987, pp. 55-64.

6. Ross, James C., "Aerodynamic Design of a Rigid-Wing Sail for a C-Class Catamaran," *SailTech - 89: Proceedings of the Eighteenth Annual Conference on Sailing Technology*, Alan J. Adler, ed. Western Periodicals Co., 1989, pp. 17-27.

7. Avila, Matthew R., *Computational and Experimental Investigation of the Aerodynamic Characteristics of a Windsurfing Sail Section*, Naval Postgraduate School, Monterey, CA, 1992.

8. Hoyt, Gary, "A Recipe for Speed," *Sailing World*, Vol. XXXV, No. 1, January, 1996, pp. 26-27.

9. Leonard, Zach, "Invention, Technology, and Audacity," *Sailing World*, Vol. XXXV, No. 1, January, 1996, pp. 34-37.

10. Le Roux, Guy, "A Tale of Boom, Bust, and Boardsailing," *Sailing World*, Vol. XXXV, No. 3, March, 1996, pp. 51-53.

11. Purtell, L. Patrick, "Turbulence: A Roadblock to Computational Fluid Dynamics," *Naval Research Reviews*, Vol. XLVII, No. 2, 1995, pp. 20-25.

12. Meldner, Heiner W., "USA'S revolutionary Appendages and CFD," *The Ancient Interface XVII: Proceedings of the Seventeenth AIAA Symposium on the Aero/ Hydronautics on Sailing*, William Feiereisen, ed. Western Periodicals Co., 1987, pp.1-6.

13. Merkle, Charles L., *Computational Fluid Dynamics of Inviscid and High Reynolds Number Flows*, Charles L. Merkle, 1990.

14. Buning, P. G., and others, *OVERFLOW User's Manual Version 1.6aw*, NASA Ames Research Center, California, July, 1995.

15. Ekaterinaris, John A., "Program: ns_pot," NASA Ames Research Center, California, March, 1990, modified by Tuncer, I. H., Naval Postgraduate School, April, 1992.

16. Steinbrenner, J. P., and Chawner, J. R., *GRIDGEN Release Notes Version 9.6*, MDA Engineering, Arlington, Texas, October, 1994.

17. *Flow Analysis Software Toolkit Version 1.1a - FAST*, Numerical Aerodynamics Simulation Division, NASA Ames Research Center.

18. Walatka, P. P., and Buning, P. G., *PLOT3D User's Manual Version 3.5*, NASA Ames Research Center, California, 1989.

APPENDIX A. WIND CALCULATIONS

Atmospheric Boundary Layer Wind Calculations

Close Reach						Broad Reach					
Vb	30	gamma	143.5°	Vt(30)=	48	Vb	30	gamma	90°	Vt(30)=	30
	z (ft)	Vt (Kts)	Va (Kts)	Beta			z (ft)	Vt (Kts)	Va (Kts)	Beta	
	0	0	30	0			0	0	30	0	
	0.25	38.2970	22.7935	91.9745			0.25	23.9356	38.3785	38.5848	
	0.5	40.32	24.1041	95.7417			0.5	25.2	39.1795	40.0302	
	0.75	41.5033	24.9151	97.7567			0.75	25.9395	39.6593	40.8484	
	1	42.3429	25.5081	99.1075			1	26.4643	40.0045	41.4169	
	1.25	42.9941	25.9774	100.112			1.25	26.8713	40.2749	41.8511	
	1.5	43.5262	26.3666	100.906			1.5	27.2039	40.4975	42.2016	
	1.75	43.9761	26.6996	101.560			1.75	27.4850	40.6869	42.4949	
	2	44.3658	26.9907	102.113			2	27.7286	40.8519	42.7468	
	2.25	44.7095	27.2496	102.590			2.25	27.9434	40.9980	42.9673	
	2.5	45.0170	27.4827	103.010			2.5	28.1356	41.1292	43.1632	
	2.75	45.2952	27.6948	103.384			2.75	28.3095	41.2483	43.3393	
	3	45.5491	27.8895	103.720			3	28.4682	41.3574	43.4992	
	3.25	45.7827	28.0694	104.025			3.25	28.6142	41.4581	43.6456	
	3.5	45.9990	28.2367	104.304			3.5	28.7494	41.5515	43.7805	
	3.75	46.2004	28.3930	104.561			3.75	28.8752	41.6386	43.9055	
	4	46.3887	28.5398	104.799			4	28.9929	41.7204	44.0220	
	4.25	46.5656	28.6781	105.020			4.25	29.1035	41.7973	44.1310	
	4.5	46.7325	28.8088	105.226			4.5	29.2078	41.8699	44.2334	
	4.75	46.8903	28.9329	105.420			4.75	29.3064	41.9388	44.3299	
	5	47.04	29.0509	105.602			5	29.4	42.0042	44.4212	
	5.25	47.1823	29.1634	105.774			5.25	29.4889	42.0666	44.5078	
	5.5	47.3181	29.2709	105.936			5.5	29.5738	42.1261	44.5901	
	5.75	47.4478	29.3738	106.090			5.75	29.6549	42.1831	44.6685	
	6	47.5720	29.4726	106.237			6	29.7325	42.2377	44.7434	
	6.25	47.6912	29.5675	106.377			6.25	29.8070	42.2901	44.8151	
	6.5	47.8056	29.6588	106.510			6.5	29.8785	42.3406	44.8838	
	6.75	47.9158	29.7469	106.638			6.75	29.9474	42.3892	44.9497	
	7	48.0219	29.8319	106.760			7	30.0137	42.4361	45.0131	

APPENDIX B. OVERFLOW INPUT FILE

```
$GLOBAL
    CHIMRA= .F., NSTEPS= 2000, RESTRT= .F., NSAVE = 10,
    NQT = 0,
    $END
$FLOINP
    ALPHA = 6.0, BETA = 0.0, FSMACH = 0.2, GAMINF = 1.4,
    REY = 8.E5, TINF = 522.0,
    $END
$VARGAM
    $END
$GRDNAM
    NAME = 'Windsurfer sail (alpha 6.00 / M 0.2 / Re .8 mill)',
    $END
$NITERS
    $END
$METPRM
    IRHS = 0, ILHS = 2, IDISS = 2,
    $END
$TIMACU
    ITIME = 1, DT = 0.25, CFLMIN = 0.01,
    $END
$SMOACU
    ISPECJ = 2, DIS2J = 2.0, DIS4J = 0.02,
    ISPECK = 2, DIS2K = 2.0, DIS4K = 0.02,
    ISPECL = 2, DIS2L = 2.0, DIS4L = 0.02,
    SMOO = 1.0,
    $END
$VISINP
    VISCJ = .T., VISCK = .T., VISCL = .T.,
    NTURB =    3,
    ITTYP =    1,  11,  11,
    ITDIR =    2,   2,   2,
    JTLS  =   70,   1, -69,
    JTLE  =  -70,  69,  -1,
    KTLS  =    1,   1,   1,
    KTLE  =   -1,  -1,  -1,
    LTLS  =    2,   2,   2,
    LTLE  =   -2,  -2,  -2,
    TLPAR1=   2.,  1.,  1.,
    $END
$BCINP
    NBC   =    6,
    IBTYP =    5, 32, 32, 32, 51, 21,
    IBDIR =    2, -2,  1, -1,  2,  3,
    JBCS  =   70,  1,  1, -1,  1,  1,
    JBCE  =  -70, -1,  1, -1, 69, -1,
    KBCS  =    1, -1,  1,  1,  1,  1,
    KBCE  =    1, -1, -1, -1,  1, -1,
    LBCS  =    2,  2,  2,  2,  2,  1,
    LBCE  =   -2, -2, -2, -2, -2,  1,
    $END
$SCEINP $END
```

APPENDIX C. NS INPUT FILE

```
------------------------------------------------------------------------
C.. IREAD,     ITER     NPRINT,     NLOAD     ODVAR
    0          1000     1           1         0.10
C.. ALPHA     OSCIL     RAMP      REDFRE     ALFAMND     ALFAMXD
    14.000    false     false     0.099      0.001       16.0
C.. PLUNGE     PLMX     PLMY      PLPHSXD     PLFREQ
    false      0.       0.10      0.          1.5
C.. MACH      REYNOLD     VISC      TURBL     TRANS
    0.200     800000.     true      true      false
C.. TIMEACC     COUR     NEWTIT
    true         100.    2
C.. POTEN,     NTPOT,     MPOT,     KSISO,     SO_DIST     XWKSi
    false      1          10        4          0.20        0.30
```

APPENDIX D. 3-D MODEL SECTION PLACEMENT

Calculation of Wing-sail Twist Angles

z	wing-sail	broad reach	close reach	average	difference
(ft)	twist angle	beta angle	beta angle	wind angle	model angle
0	1.5	0	0	0	1.5
0.5	1	-5.165	-2.17139	-3.668195	4.668195
1	0.5	-1.799	-0.7847	-1.29185	1.79185
1.5	0	0	0	0	0
2.5	1.36905	2.1039	0.96159	1.532745	-0.163695
3.5	2.7381	3.3978	1.57889	2.488345	0.249755
4.5	4.10715	4.3197	2.0318	3.17575	0.9314
5.75	5.81845	5.1841	2.46693	3.825515	1.992935
6	7.25	5.3308	2.54182	3.93631	3.31369
6.5	8.75	5.604	2.68215	4.143075	4.606925

INITIAL DISTRIBUTION LIST

		No. Copies
1.	Defense Technical Information Center 8725 John J. Kingman Rd., STE 0944 Ft. Belvoir, VA 22060-6218	2
2.	Dudlley Knox Library Naval Postgraduate School Monterey, CA 93943-5101	2
3.	Prof. D. J. Collins, Chairman, Code AA/Co Department of Aeronautics and Astronautics Naval Postgraduate School Monterey, CA 93943-5106	1
4.	Prof. G. Hobson, Code AA/Hg Department of Aeronautics and Astronautics Naval Postgraduate School Monterey, CA 93943-5106	5
5.	Prof. R. Howard, Code AA/Ho Department of Aeronautics and Astronautics Naval Postgraduate School Monterey, CA 93943-5106	1
6.	Louis Partida 5840 Blueberry St. Yorba Linda, CA 92686	2